

First-principle studies of the initiation  
mechanism of energetic materials

Thesis by  
Wei-Guang Liu

In Partial Fulfillment of the Requirements for the degree  
of  
Doctor of Philosophy



CALIFORNIA INSTITUTE OF TECHNOLOGY  
Pasadena, California  
2014  
(Defended December 19, 2013)

*To my family*

© 2014

Wei-Guang Liu

All Rights Reserved

## ACKNOWLEDGEMENTS

I would like to express my sincere gratitude to my advisor, Dr. William A. Goddard III, who has been very supportive and patient in guiding me throughout my six years at Caltech. To me, the best thing about being his student is that I can always pick interesting problems to work on. Because there are so many different and diverse research topics in his group, like an all-you-can-eat buffet, and I am the person who enjoyed the feast for six years yet still have not tasted all dishes on the table. It is very enjoyable to discuss with Bill because of his broad knowledge and bold ideas. I have learned a lot from him.

I would also like to thank my thesis committee members: Dr. Rudolph A. Marcus, Dr. Nathan S. Lewis, and Dr. Thomas F. Miller III for their advice. It is a great honor to have brilliant scientists as my committee members. I appreciate their comments and advice on my exams.

I would like to thank many people in my group. Dr. Robert Nielson introduced me to the world of organometallics. Dr. Julius Su taught me his creative eFF and molecular dynamics when I was new to the group. Dr. Sergey V. Zybin and Dr. Siddharth Dasgupta introduced me the study of energetic material. Many thanks to my colleagues: Ted Yu, Mu-Jeng Cheng, Tod Pascal, Jonathan Muller, Amos Anderson, Yuki Mazda, Qi An., Caitlin Scott, Jose Mendoza-Cortes, Hai Xiao, Fan Liu, Himenshu Mishra, Jason Crowley, Ho-Cheng Tsai, Ross Fu and many other people in the group. They enriched my life in the lab and I appreciate all discussions with them.

I would like to thank my collaborators: Penn State group, Dr. Stefan T. Thynell and Dr. Shiqing Wang, who carried out the experimental work in the project of hypergolic fuel. Dr. Thomas M. Klapötke, who synthesizes many interesting yet dangerous materials. Northwestern group: Dr. Fraser Stoddart, Dr. Marco Frasconi, Michal Juricek, Jonathan Barnes, and Hao Li. They synthesize all

wonderful molecular machines. Maryland group: Dr. Andrei N. Vedernikov and Anna Vladimirovna Sbergaeva. They carried out the experimental work of methane activation. Thanks to Agustin J. Colussi for his experiments about NO<sub>2</sub> dimerization on the surface.

Last but not least, I would like to thank my family in Taiwan. They are very supportive of my choice to pursue a PhD degree. I thank Tzu-Yi Yang, my girlfriend, for her patience to the long-distance relationship. I would also like to thank many Taiwanese friends here: I-Ren Lee, Jen-Kan Yu, Wei-Chen Chen, Chun-Hui Lin, Hsi-Chun Liu, Chien-Yao Tseng, Hsin-Hua Lai, Yun Mou, Yun-Hua Hong, Chih-Kai Yang, Chih-Hao Liu, Han-Chieh Chang and many other friends. They are not only good for sharing my happiness, but also never hesitate to give a hand when I need help. With these friends, my six years here is very joyful.

## ABSTRACT

It is important to understand the initiation mechanism of energetic materials to improve and engineer them. In this thesis, first-principle calculation is used to study the initiation of several explosives and propellants.

The second chapter is focused on a new energetic material, silicon pentaerythritol tetranitrate (Si-PETN), DFT calculations have identified the novel rearrangement that explains the very dramatic increase in sensitivity observed experimentally. The critical difference is that Si-PETN allows a favorable five-coordinate transition state in which the new Si-O and C-O bonds form simultaneously, leading to a transition state barrier of 33 kcal/mol (it is 80 kcal/mol for PETN) and much lower than the normal O-NO<sub>2</sub> bond fission observed in other energetic materials (40 kcal/mol). In addition this new mechanism is very exothermic (45 kcal/mol) leading to a large net energy release at the very early stages of Si-PETN decomposition.

The third chapter is about nitrogen-rich compounds, which has high heat of formation and releases the energy by decomposing into stable N<sub>2</sub> molecules. Two families of compounds, azobistetrazoles and azobistriazoles, were studied. Based on the calculated mechanisms, for azobistetrazoles with four N atoms in the five-member ring, a clearly-defined N=N fragment can always be found in the ring, and its decomposition starts with ring-opening to free one end of N=N followed by N<sub>2</sub> dissociation and heat generation. This barrier is around 28-35 kcal/mol, which is low enough to dominate the sensitivity of material. For azobistriazoles, only 1,1'-azobis-1,2,3-triazole has a N=N fragment in the original 5-member ring and similar ring-opening - N<sub>2</sub> dissociation pathway is favored.

For the remaining compounds, an additional isomerization is necessary to release  $N_2$ , which gives the barrier around 55~60 kcal/mol, making these compound less sensitive.

The fourth chapter shifts focus to hypergolic propellants. DFT calculations with B3LYP functional was applied to study the hypergolic reaction between N,N,N',N'-tetramethylethylenediamine (TMEDA), N,N,N',N'-Tetramethylmethylenediamine (TMMDA) and  $HNO_3$ . Bond energies in TMEDA and TMMDA were calculated and compared with their alkane analogues to demonstrate that the lone-pair electrons on N atoms plays the role of activating adjacent chemical bonds. Two key factors relating to the ignition delay were calculated at atomistic level. The first factor is the exothermicity of the formation of the dinitrate salt of TMEDA and TMMDA. Because of the shorter distance between basic amines in TMMDA, it is more difficult to protonate both amines for the stronger electrostatic repulsion, resulting in the smaller heat of dinitrate salt formation by 6.3kcal/mol. The second factor is the reaction rate of TMEDA and TMMDA reacting with  $NO_2$  to the step that releases enough heat and more reactive species to propagate reaction. In TMEDA, the formation of the intermediate with C-C double bond and the low bond energy of C-C single bond provide a route with low barrier to oxidize C. Both factors can contribute to the shorter ignition delay of TMEDA.

The fifth chapter is about the other pair of hypergolic propellant, monomethylhydrazine (MMH) with oxidizers  $NO_2/N_2O_4$ . Experimentally several IR-active species were identified in the early reactions, including HONO, monomethylhydrazinium nitrite (MMH•HONO), methyl diazene ( $CH_3N=NH$ ), methyl nitrate ( $CH_3ONO_2$ ), methyl nitrite ( $CH_3ONO$ ), nitromethane ( $CH_3NO_2$ ), methyl azide ( $CH_3N_3$ ),  $H_2O$ ,  $N_2O$  and  $NO$ . In order to elucidate the mechanisms by which these

observed products are formed, we carried out quantum mechanics calculations (CCSD(T)/6-31G\*\*//M06-2X/6-311G\*\*++) for the possible reaction pathways. Based on these studies, we proposed that the oxidation of MMH in an atmosphere of  $\text{NO}_2$  occurs via two mechanisms: (1) sequential H-abstraction and HONO formation, and (2) reaction of MMH with asymmetric  $\text{ONONO}_2$ , leading to formation of methyl nitrate. These mechanisms successfully explain all intermediates observed experimentally. We concluded that the formation of asymmetric  $\text{ONONO}_2$  is assisted by an aerosol formed by HONO and MMH that provides a large surface area for  $\text{ONONO}_2$  to condense, leading to the generation of methyl nitrate. Thus, we proposed that the overall pre-ignition process involves both gas-phase and aerosol-phase reactions.

The sixth chapter is about another pair of hypergolic propellant, unsymmetrical dimethylhydrazine (UDMH) with oxidizers  $\text{NO}_2/\text{N}_2\text{O}_4$ . We carried out the same level of quantum mechanics calculations as MMH to study this pair. We proposed that the oxidation of UDMH in an atmosphere of  $\text{NO}_2$  occurs via two mechanisms, similar with MMH: (1) sequential H-abstraction and HONO formation in gas phase, which has no more than 20 kcal/mol barrier and leads to the production of  $(\text{CH}_3)_2\text{NNO}$  and HONO. (2)UDMH reacts with asymmetric  $\text{ONONO}_2$  in aerosol phase, leading to formation of  $\text{CH}_3\text{N}_3$  and then  $\text{CH}_3\text{ONO}_2$ , with a 26.8 kcal/mol enthalpic barrier, which is 10 kcal/mol higher than the corresponding reaction barrier for MMH. Thus we predicted the low production rate of  $\text{CH}_3\text{ONO}_2$  for UDMH/ $\text{NO}_2$  pair. Experimental evidences support our mechanisms for both MMH and UDMH reacting with  $\text{NO}_2$ .

## TABLE OF CONTENTS

Acknowledgements .....	iii
Abstract.....	v
Table of Contents .....	viii
List of Illustrations and/or Tables .....	ix
Chapter I: Introduction to Energetic Materials.....	1
Chapter II: Explanation of the Colossal Detonation Sensitivity of Silicon Pentaerythritol Tetranitrate Explosive .....	8
Overview.....	8
Computational methods.....	9
Results and discussion.....	9
Conclusion .....	13
References.....	14
Chapter III: First-Principles Study of the Initial Decomposition of Azobistetrazole and Azobistriazole .....	16
Overview.....	16
Computational methods.....	17
Results and discussion.....	18
Conclusion .....	23
References.....	24
Chapter IV: First Principles Study of Ignition Mechanism of Hypergolic Bipropellant: N,N,N',N'-Tetramethylethylenediamine (TMEDA), N,N,N',N'- Tetramethylmethylenediamine (TMMDA) and Nitric Acid.....	27
Overview.....	27
Computational methods.....	30
Results and discussion.....	30
Conclusion .....	44
References.....	45
Chapter V: Theoretical Investigations of Early Reactions of Monomethylhydrazine with Mixtures of NO <sub>2</sub> and N <sub>2</sub> O <sub>4</sub> .....	47
Overview.....	48
Computational methods.....	50
Results and discussion.....	51
Conclusion .....	61
References.....	61
Chapter VI: Theoretical Investigations of Early Reactions of Unsymmetrical Dimethylhydrazine with Mixtures of NO <sub>2</sub> and N <sub>2</sub> O <sub>4</sub> .....	65
Overview.....	65
Computational methods.....	66
Results and discussion.....	67
Conclusion .....	70
References.....	71

## LIST OF ILLUSTRATIONS AND TABLES

<i>Number</i>	<i>Page</i>
Table 2-1 .....	9
Figure 2-1 .....	9
Figure 2-2 .....	10
Figure 2-3 .....	11
Figure 2-4 .....	11
Figure 2-5 .....	12
Table 2-2 .....	13
Table 3-1 .....	18
Figure 3-1 .....	19
Figure 3-2 .....	21
Figure 4-2 .....	34
Figure 4-1 .....	27
Table 4-1 .....	32
Figure 4-3 .....	35
Figure 4-4 .....	36
Figure 4-5 .....	40
Figure 4-6 .....	41
Figure 4-7 .....	43
Figure 4-8 .....	44
Figure 5-1 .....	51
Figure 5-2 .....	54
Figure 5-3 .....	56
Figure 5-4 .....	57
Figure 5-5 .....	59
Figure 5-6 .....	60
Figure 6-1 .....	66
Figure 6-2 .....	67
Figure 6-3 .....	68
Figure 6-4 .....	69

## *Chapter 1*

### INTRODUCTION TO ENERGETIC MATERIALS

Energetic materials are a class of material that can release chemical energy stored in their molecular structure. Upon external stimulations, such as heat, shock, or electrical current, these materials will emit energy in a short time.<sup>1</sup> The earliest record of energetic material can be traced back to the text written in the 6th century by the Chinese alchemist Sun Simiao, in which the combustion of the powder mixture of sulfur and nitrate salts was described.<sup>2</sup> Later the invention was modified and applied in the war between the Song dynasty and Mongols. In 1867, Alfred Nobel invented and commercialized dynamite, a mixture of nitroglycerin and silica, which was more stable and safer to use, leading to its high demand in the First World War. Although firstly known for its military application, today energetic materials are used more in fields of civil engineering and space exploration, such as mining, construction, and rocket propelling.<sup>3</sup> Even with a long history of development, people are still seeking for safer, more powerful, and more cost-effective energetic materials. To make a knowledge-based improvement and engineering, it is the first priority to understand the chemistry of energetic materials. However, the fast reaction rate and extreme reaction conditions make direct experimental measurement difficult. Developing the knowledge through computer simulation provides a safer and convenient way to study the chemistry of energetic material. In this thesis first-principle calculation is used to study the initiation of several different energetic materials.

Based on their applications, energetic materials can be classified as explosives, propellants, and pyrotechnics. The first two are discussed in this thesis and shortly introduced here.

- Explosives:

Explosives are expected to release large energy and expand greatly in volume to generate force in the time scale of  $\mu\text{s}$ . To achieve high power output, it is necessary to propagate reaction rapidly through the whole material, as known as detonate. Detonation, deflagration, and regular fuel combustion are different phenomena distinguished by their rate-determining-step and propagation rate. For regular fuel combustion, the reaction rate is limited by diffusion of reactive species (mass transfer), which is relatively slow, leading to low propagation rate. In the case of deflagration, the oxidizer and fuel are premixed, therefore the diffusion of reactive species is no longer the rate-determining-step. Instead, the propagation of reaction zoom is controlled by heat transfer, resulting in its faster rate than regular fuel combustion. When energetic material detonates, the shockwave propagates through the material. At the wave front the material is highly compressed, leading to the temperature rise, which triggers exothermic chemical reactions and create a chemical reaction zoom after the wave front. The exothermic reactions increase the temperature and pressure to the point higher than the condition before the passage of shock wave, which provide energy to sustain the propagation of shock wave. Therefore detonation is in the speed of shock wave, which is supersonic, in contrast to the cases of deflagration and regular fuel combustion, which are subsonic.

Several parameters can be used to characterize explosives, as described below.

i) Sensitivity:

This represents how easily the explosives can be set off by external stimulus, such as impact, friction, shock, spark, and heat. Based on their sensitivity, explosives can be categorized into primary and secondary explosives. Primary explosives are highly sensitive and easy to undergo the deflagration-to-detonation transition (DDT). On the other hand, secondary explosives, or high explosives are less sensitive, but usually more powerful. A common way to take advantage of both explosives is to place a small amount of primary explosive adjacent to a large amount of secondary explosive, or so called

explosive trains. The fast DDT of primary explosive helps to amplify the initial non-explosive impulse to shockwave, which then detonates secondary explosive.

ii) Heat of explosion ( $Q$ )

This represents the amount of heat released from the decomposition of explosive during explosion. This quantity can be well approximated as the difference of the heat of formation of combustion products and explosive itself. Large heat of formation is preferred for explosives because it leads to higher explosive power, which is defined as the product of heat of formation and the volume of gas product.

iii) Detonation velocity ( $D$ )

This quantity represents how fast the detonation wave propagates and therefore controls the rate of energy release of explosives. The value of detonation velocity increases with the density of packing of explosives in the column and is positively correlated with the detonation pressure. For most applications, such as rock cleaving and grenade, it is desirable for explosives to reach its peak pressure quickly to maximize the shattering power, and high velocity of detonation is necessary. The shattering power can be quantified by brisance, which is defined as the product of the loading density, the detonation velocity, and the specific energy (the maximum pressure through explosion multiplies volume of detonation gases).

There are many factors that determine the practicality of explosives. For the primary explosives, a fast deflagration-to-detonation transition is the requirement to be able to generate the shock wave to initiate the detonation of the secondary explosives. Despite their high sensitivities, the chemical and thermal stability of primary explosives are still necessary to have longer shelf life. Historically, heavy metal salts, such as mercury fulminate, lead azide and lead styphnate, have been used as the primary explosive. Their combustion products are hazardous if breathed in and cause the environment

pollution, leading to a need to seek for metal-free primary explosives. For the secondary explosives, besides the performance requirements (high detonation velocity and large heat of explosion), it is very important to have low sensitivity and long term stability, which make it easier to store and handle these explosives in large amounts. The production cost is another important issue to determine if one kind of explosive is practical or not.

- Propellants:

Propellants are not expected to detonate, but combust in a controlled manner, i.e., DDT is not desired for propellants, different than explosives. The most important performance parameter of propellants is specific impulse ( $I_{sp}$ ), which is defined as the gain of impulse (impulse=force  $\times$  time, or mass  $\times$  velocity)<sup>4</sup> when one unit mass of propellants is consumed, and it can be roughly perceived as the exhaust velocity. Since  $I_{sp}$  is normalized to per unit mass, it is a material-specific parameter and not dependent on the burning rate of propellant if the thrust comes from only the exhaust gas.

Propellants can be in liquid or solid form. Common solid propellants are mixtures of oxidant (nitrate or perchlorate salts) and reductant powder (C, Al, etc.). Explosives, such as RDX or HMX, can also be used as propellants, as long as there is no shockwave generated during the combustion to start the detonation. Rocket motors powered by solid propellants have high propellant fraction in weight because there is no liquid pump or cryogenic tank, and they are more reliable to operate. The drawback is that once the motor starts, there is little control over the combustion of the solid propellants.

Liquid propellants can be further categorized into monopropellants and bipropellants. Common monopropellants, such as hydrogen peroxide and hydrazine, are able to decompose catalytically to release gas products and heat. However their  $I_{sp}$  are not as high as bipropellants, and this is usually due to their smaller  $\Delta H$ . Thus, monopropellants they are only applied on missions with small loading.

Bipropellants include oxidizer and fuel that are injected and mixed in the combustion chamber. One important type of bipropellants is hypergolic propellants, which are pairs of fuel and oxidizer that ignite spontaneously upon mixing. They facilitate the design of rocket thrusters by simplifying the ignition system, and are widely used in propulsion systems in which variable and/or intermittent thrust capabilities are needed. Besides  $I_{sp}$ , the most important parameter of hypergolic propellant is ignition delay, which is defined as the time interval from the touch of two liquid surfaces to the flame appearance. Shorter ignition delay implies faster response and easier motion control. Hydrazine and its derivatives, such as monomethylhydrazine (MMH) and unsymmetrical dimethylhydrazine (UDMH) are commonly used hypergolic fuels combining with  $\text{HNO}_3$  or nitrogen tetroxide (NTO) as oxidizer. However hydrazine derivatives are carcinogens and to replace them with safer fuels, such as alkylamines, is desirable.

At atomistic level, the initiation of energetic material involves two processes, molecule activation and energy propagation, which form a positive feedback loop. Starting with the cold, unreacted material, the external stimuli drive molecules in ground state going over barriers. At the condition that stimuli are not too strong, only low-lying reaction channels are activated. As these reactions proceed, some of them are exothermic and raise the local temperature. The heat and mechanical energy propagate to neighboring unreacted molecules as the external stimuli and repeat the process. In the above mechanism there are three factors affecting propagation rate of reaction zoom: 1.) the barrier height of reactions, which controls the accessibility of reaction channels, 2.) the exothermicity of reactions, which associates with the amount of heat that is released to raise the local temperature, and 3.) the efficiency of energy transfer to neighbor molecules. The energy can be transferred via the coupling of vibrations between adjacent molecules or via the momentum carried by ballistic gas molecules generated and accelerated in the exothermic, gas-releasing reactions. These three factors determine the sensitivity of energetic materials, as one or more highly exothermic channels with low barrier height will lead to the high sensitivity.

It is possible to theoretically characterize the overall combustion process of energetic material via multi-paradigm multi-scale simulations. Firstly the reaction mechanism, such as the barrier height and exothermicity of unimolecular or bimolecular reactions starting from the unreacted molecule can be constructed with first-principle based methods. Based on these reaction mechanisms and potential energy surfaces, one can develop force field for the simulation of molecular dynamics (MD), which can be applied to study multimolecular process such as energy transfer between molecules and reactions occurring in condense phase. Finally, one can construct a combustion model containing rate constant and exothermicity of reactions for all species based on MD simulation results. The model can describe the time-evolution of all species and when combined with continuum fluid dynamics (CFD), a detailed simulation of engine operation including macroscopic phenomena, such as diffusion and heat transfer, can be achieved.

The focus of this thesis is to use first-principle method to develop the early reaction mechanisms of different energetic materials, where the temperature is still low and channels involving direct bond-fission are not accessible. Such mechanisms at the early stage are important to determine the sensitivity and initiation of energetic materials. In the second chapter, a newly synthesized, Si-based explosive, Si-PETN, is studied. Its colossal sensitivity is found to be correlated to a particular reaction path that is with low barrier and high exothermicity. The third chapter studies the decomposition mechanism of a new class of energetic material, azobis(tetrazole) and azobis(triazole), which contain very high percentage of nitrogen. The fourth chapter discusses the reaction mechanism of two hypergolic fuel and oxidizer pairs, N,N,N',N'-tetramethylethylenediamine (TMEDA) and N,N,N',N'-tetramethylmethylenediamine (TMMDA) with nitric acid. The difference in their ignition delays is explained based on the reaction mechanism and the exothermicity for formation of the dinitrate salt from TMEDA or TMMDA. The fifth chapter studies the reaction mechanisms of hypergolic pair,

MMH/NTO. The sixth chapter covers the other hypergolic pair, UDMH/NTO, in the preignition environment. The gas products were found to consistent with the experimental results.

**References:**

1. Millar, D. I. A., *Energetic Materials at Extreme Conditions*. Springer Berlin Heidelberg: 2012.
2. Deng, Y., *Ancient Chinese Inventions*. Cambridge University Press: 2011.
3. Singh, R. P.; Verma, R. D.; Meshri, D. T.; Shreeve, J. M., *Angew. Chem., Int. Ed.* **2006**, *45* (22), 3584-3601.
4. Klapötke, T. M., *Chemistry of High-energy Materials*. De Gruyter: 2011.

## Chapter 2

### EXPLANATION OF THE COLOSSAL DETONATION SENSITIVITY OF SILICON PENTAERYTHRITOL TETRANITRATE EXPLOSIVE

#### Overview

For applications requiring high shattering power, it is desirable to increase detonation velocity so the energy can be released faster to achieve higher power output. One way to achieve this goal is to increase the density of energetic material. Based on this idea, a new silicon-based explosive was recently synthesized by the nitration of tetrakis(hydroxymethyl)-silane,  $\text{Si}(\text{CH}_2\text{OH})_4$ , with nitric acid<sup>1</sup>. This sila-pentaerythritol tetranitrate (Si-PETN),  $\text{Si}(\text{CH}_2\text{ONO}_2)_4$  (tetrakis(nitratomethyl)-silane) has a molecular structure nearly identical to its carbon analog - pentaerythritol tetranitrate (PETN),  $\text{C}(\text{CH}_2\text{ONO}_2)_4$  - with the central carbon atom replaced by silicon, resulting in higher density than the original PETN. Unexpectedly, Si-PETN shows dramatically increased sensitivity, exploding with just a touch of a spatula (no impact), more sensitive than mercury fulminate and far more sensitive than PETN, making it extremely dangerous and difficult to study. Detonation sensitivity is an extremely important issue in explosives, involving many factors, such as the crystal orientation and morphology<sup>2,3</sup>, hot spot formation<sup>4-6</sup>, bandgap<sup>7</sup>, and the distribution of electrostatic potential<sup>8,9</sup>. However, there is no clear understanding about the molecular and structural determinants controlling their sensitivity to external stimuli. Since the molecular structures of PETN and Si-PETN are very similar with very similar contacts between various molecules in the crystal, we considered that elucidating how replacing the central C with Si dramatically increases sensitivity might provide clues useful for understanding sensitivity in other systems. In this chapter I carried out DFT calculations on pathways for unimolecular decomposition and showed that there exists a unique pathway that differentiates PETN and Si-PETN, which suggests an explanation of the colossal sensitivity.

## Computational methods

All calculations were carried out with Jaguar 7.0 package<sup>10</sup>, using the unrestricted hybrid functional UB3LYP<sup>11</sup> and UM06<sup>12</sup> to locate all the stationary points and to calculate Hessian matrix for zero point energy and reaction enthalpy at 6-311G\*\* level. Data in the Table 2.1 for small nitrate esters show that B3LYP tends to underestimate the O-N Bond Dissociation Energy (BDE) by ~ 5 kcal/mol, in agreement with previous calculations<sup>13</sup>, while the M06 functional generally reproduces the experimental BDEs<sup>14</sup>. Thus M06 leads to a BDE for reaction 1 (see Figure 2.1) in PETN of 39.0 kcal/mol, within the range of experimental values of 35.0<sup>15</sup>, 39.5<sup>16</sup> and 45.9<sup>17</sup> kcal/mol. Consequently we will quote only the M06 values below.

**Table 2.1** Comparison of B3LYP and M06 for various bond energies (in kcal/mol). We conclude that the M06 is more accurate.

O-N BDE	B3LYP	M06	Experiment <sup>6</sup>
Methyl-nitrate	35.5	42.5	41.2±1.0
Ethyl-nitrate	34.1	42.1	41.0±1.0
propyl-nitrate	36.2	44.3	42.3±1.0
Iso-propyl-nitrate	36.0	44.2	41.1±1.0
C-O BDE	B3LYP	M06	Experiment
Methyl-nitrate	75.0	83.6	81.0±1.0

## Results and discussion

Five different reaction pathways were studied, as shown in the Figure 2-1. NO<sub>2</sub> dissociation (reaction 1) generally provides the lowest barrier for unimolecular decomposition of energetic materials with nitro group, such as RDX<sup>18</sup>, PETN<sup>15-9</sup>, and HMX<sup>19</sup> although HONO elimination (reaction 3) is

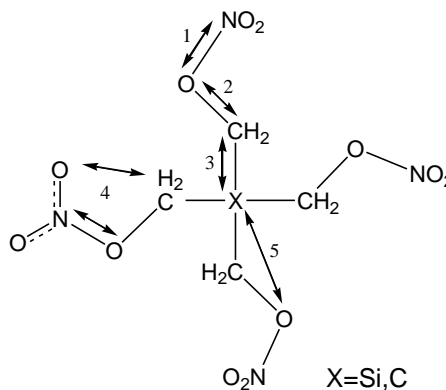


**Figure 2-1.** The structure of PETN (X=C) and SiPETN (X=Si) and five reactions studied in this work.

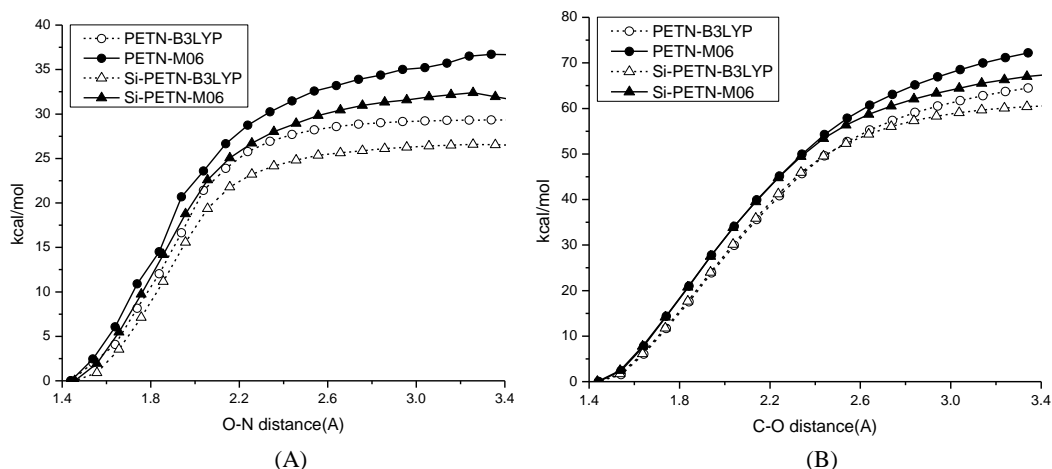


**Figure 2-2** (A) O-N bond (B) C-O bond scan by B3LYP and M06 at 6311G\*\* level. Zero point energies are included.

often close. The calculated O-NO<sub>2</sub> BDEs are 39.0 kcal/mol for PETN and 35.6 kcal/mol for Si-PETN. The O-N bond scans are shown in Figure 2-2A. This lower O-N bond energy of Si-PETN may facilitate the propagation of chain reactions to contribute partially to its sensitivity. However, this reaction is not exothermic and it is *not* the decomposition pathway with the lowest barrier, as discussed below.

The C-O bond-breaking (reaction 2) leads to BDE = 82.2 (C) and 77.6 (Si), as shown in Figure 2-2B. With such high barriers, they would only be observed in high energy laser experiments<sup>20</sup> and would not explain the difference in sensitivity.

The potential energy surface near the transition state to break the X-C bond (reaction 3) is very flat (see Figure 2-3), making it difficult to locate the precise transition state. Consequently, we carried out a 2-D scan of the X-C and O-NO<sub>2</sub> bond lengths, which shows that the central Si-C bond of Si-PETN and C-C bond of PETN are strongly dependent on the O-NO<sub>2</sub> bond. Stretching the O-NO<sub>2</sub> bond weakens the X-C bond because the oxygen forms a C=O double bond by withdrawing electron density from the X-C bond. The product of this reaction is CH<sub>2</sub>O, NO<sub>2</sub>, and a tertiary C/Si free radical. The lower electronegativity of Si (1.8) compared to C (2.5), explains the drastically different charges on the central atoms: -0.19 in PETN +0.25 in Si-PETN (B3LYP, with similar

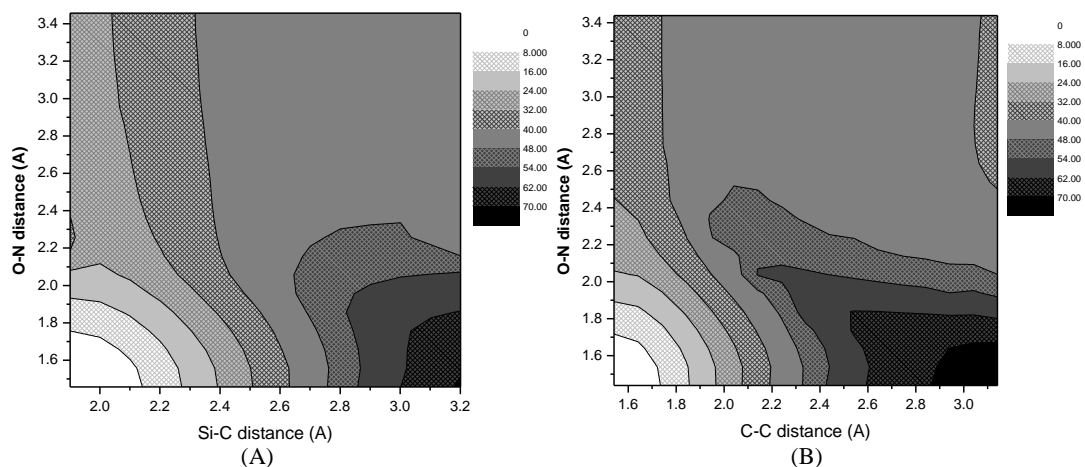


**Figure 2-3** Two dimensional scans of (A) Si-C and O-N bond of Si-PETN (B) C-C and O-N bond of PETN by B3LYP at 6311G\*\* level.

trends from M06). However the similar transition state (TS) barriers of 51.3 kcal/mol (C) and 49.7 kcal/mol (Si) would not explain the difference in sensitivity.

Next we examined HONO dissociation (reaction 4) involving simultaneous formation of a new OH bond with breaking of the O-NO<sub>2</sub> bond, as shown in Figure 2-4. This is a well known mechanism for energetic molecules with the nitro group, discovered first in DFT calculations<sup>18</sup>, which leads to an activation energy of 39.2 kcal/mol for RDX<sup>18</sup> and 44.6 kcal/mol for HMX<sup>19</sup>. For PETN this

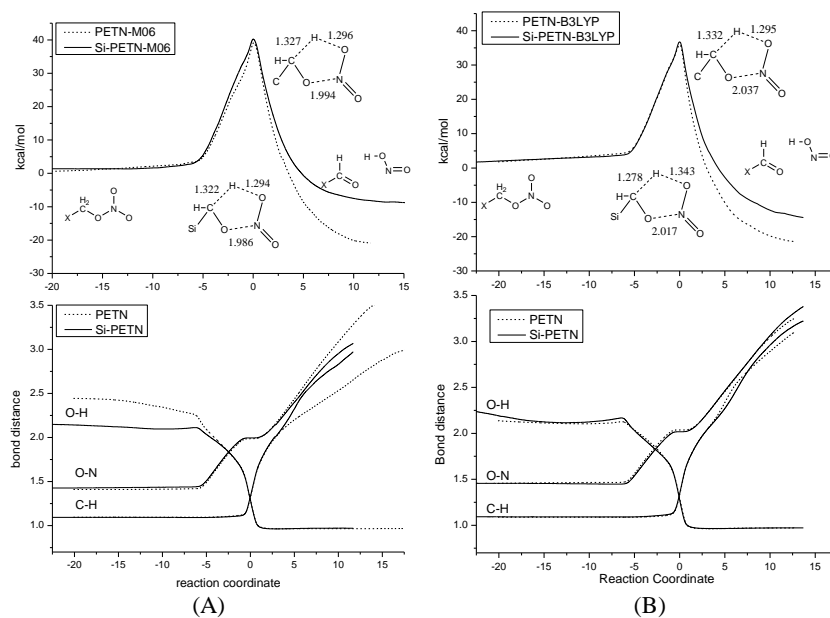


**Figure 2-4** HONO dissociation pathway of PETN and SiPETN by (A) M06 (B) B3LYP

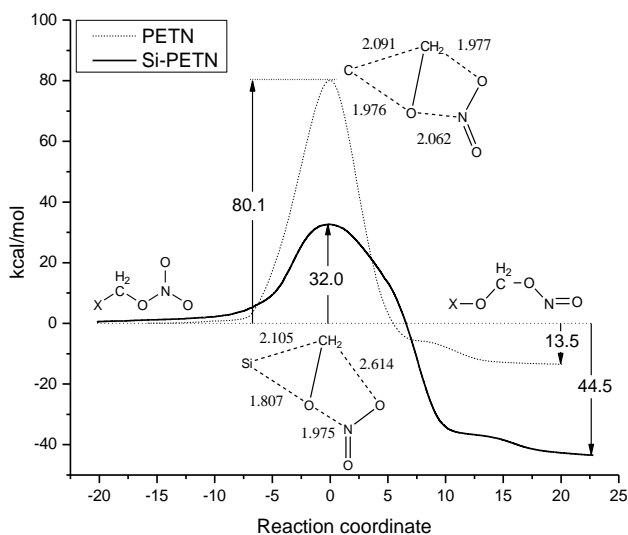


**Figure 2-5.** Energy vs. reaction coordinate and the geometry of the transition state (from DFT at the M06/6-311G\*\* level). The IRC step is 0.1 a.u. with mass-weighted coordinate.

PETN is formed by bending the C-ONO<sub>2</sub> angle, breaking the partial Si-C bond, and making Si-O bond concurrently, as shown in Figure 2-5. This was studied by first locating the transition structure through 2-D scans followed by intrinsic reaction coordinate (IRC) scans. We find that Si-PETN has a 32.0 kcal/mol barrier for this rearrangement, which is dramatically *lower* than the value of 80.1 kcal/mol for PETN. This is partly due to the larger size of silicon (Si covalent radius of 1.17 Å compared to 0.771 Å for C<sup>21</sup>) resulting in a more stable five-coordinate transition state in Si-PETN, allowing the Si-C bond and Si-O bond to be shorter with the O-N bond broken later thereby decreasing the energy barrier significantly. Besides, Si is more electropositive than C, resulting in larger Si-O bond energy and therefore lower barrier for this rearrangement. Murray et al.<sup>22</sup> applied reaction force analysis and found that most of the difference between the rearrangement barriers for PETN and Si-PETN is that Si-PETN benefits from a 1,3 electrostatic interaction involving a positive sigma-hole on the silicon and the negative linking oxygen, leading to the same conclusion.

An additional important factor in detonation sensitivity and a second dramatic difference between PETN and Si-PETN is the heat release which is 44.5 kcal/mol exothermic for reaction 5 with Si-

leads to TS energies of 39.2 (C) and 39.4 (Si), very similar to reaction 1. Such a tiny difference would not explain the huge difference in sensitivity.

Finally we considered the attack of the  $\gamma$  O on the  $\alpha$  central C/Si atom, reaction 5, in which the  $\beta$  CH<sub>2</sub> group stays bonded to the  $\gamma$  O as the X-O bond forms simultaneously to a terminal O of the NO<sub>2</sub>. Thus, the transition state in Si-

PETN, whereas the favorable decomposition for PETN (reaction 1) is 39.0 kcal/mol endothermic. To estimate the difference between two exothermic reactions in Si-PETN, the corresponding unimolecular decomposition rates of reaction 4 and 5 were calculated using the transition state theory<sup>23</sup>. Assuming no tunneling, the rate of reaction 5 is  $1.6 \times 10^4$  times faster than reaction 4 at 298K (see SI), making it plausible that reaction 5 may contribute significantly to sensitivity.

This mechanism also explains the Si-NMR spectroscopy of the decomposition product from Si-PETN, which contains the signal for siloxane  $-\text{OSi}-(\text{CH}_2\text{OR}_2)\text{O}-$ . Reaction 5 is similar to the Brook rearrangement<sup>24</sup> of the silyl group in silyl alcohols from carbon to oxygen, but this analog reaction cannot reach the transition state without breaking the O-H bond leading to a calculated barrier of 83.3 kcal/mol<sup>25</sup>. In Si-PETN the  $\alpha$ -silyl alcohol is replaced by the  $\alpha$ -silyl nitro-ester and a flexible bond angle with a weak O-N bond, all of which favors the reaction 5 rearrangement product by dramatically decreasing the TS energy.

## Conclusion

DFT calculations have identified a novel carbon-oxygen rearrangement of the newly synthesized Si derivative of the PETN energetic molecule that provides a plausible explanation of the dramatic increase in sensitivity observed experimentally. The results are concluded in Table 2-2. The

**Table 2-2.** The BDE of each bond and energies of transition state. All energies in kcal/mole.

Reaction	PETN		SiPETN	
	B3LYP <sup>a</sup>	M06 <sup>a</sup>	B3LYP <sup>a</sup>	M06 <sup>a</sup>
1: O-NO <sub>2</sub> (BDE)	35.8	39.0	28.7	35.6
2: C-ONO <sub>2</sub> (BDE)	73.3	82.2	69.4	77.6
3: C-X (TS)	41.7	49.1	40.6	48.2
4: HONO (TS)	36.2	39.2	36.5	39.4
5: O-X (TS)	73.1	80.1	30.5	32.0

<sup>a</sup> Numbers listed here are DFT using the 6-311G\*\* basis set .

<sup>b</sup> The most recent experimental BDE is 39.5kcal/mol after correcting for the zero point energy correction and thermal correction to 298.15K indicating that the M06 results more accurate than B3LYP.

primary factors leading to this are the much stronger Si-O bond over C-O, the ability of the much larger Si to adopt the 5-coordinate transition state required for reaction 5, and the ability of the terminal O of NO<sub>2</sub> to stabilize this 5-coordinate transition state. In addition to the significantly lower barrier (32 vs. 80 kcal/mol), reaction 5 is also far more exothermic (45 vs. 13 kcal/mol) because a new Si-O bond is formed. This provides a large net energy release at very early stages of Si-PETN decomposition facilitating a fast temperature increase and expansion of the reaction zone. This combination of kinetic and thermodynamic enhancement factors for the Si analog illustrates a path to controlled sensitivity of other Si analogs of energetic molecules.

## References

1. Klapotke, T. M.; Krumm, B.; Ilg, R.; Troegel, D.; Tacke, R., *J. Am. Chem. Soc.* **2007**, *129* (21), 6908-6915.
2. Dick, J. J.; Mulford, R. N.; Spencer, W. J.; Pettit, D. R.; Garcia, E.; Shaw, D. C., *J. Appl. Phys.* **1991**, *70* (7), 3572-3587.
3. Czerski, H.; Proud, W. G., *J. Appl. Phys.* **2007**, *102* (11), 8.
4. Field, J. E.; Bourne, N. K.; Palmer, S. J. P.; Walley, S. M.; Smallwood, J. M., *Philosophical Transactions of the Royal Society of London Series a-Mathematical Physical and Engineering Sciences* **1992**, *339* (1654), 269-283.
5. Tokmakoff, A.; Fayer, M. D.; Dlott, D. D., *J. Phys. Chem.* **1993**, *97* (9), 1901-1913.
6. Cai, Y.; Zhao, F. P.; An, Q.; Wu, H. A.; Goddard, W. A.; Luo, S. N., *J. Chem. Phys.* **2013**, *139* (16), 164704.
7. Zhu, W.; Xiao, H., *Struct. Chem.* **2010**, *21* (3), 657-665.
8. Murray, J. S.; Lane, P.; Politzer, P.; Bolduc, P. R., *Chem. Phys. Lett.* **1990**, *168* (2), 135-139.
9. Murray, J. S.; Lane, P.; Politzer, P., *Mol. Phys.* **1995**, *85* (1), 1-8.

10. Jaguar, v., Schrödinger, LLC, New York, NY, **2007**.
11. Lee, C. T.; Yang, W. T.; Parr, R. G., *Physical Review B* **1988**, *37* (2), 785-789.
12. Zhao, Y.; Truhlar, D. G., *Acc. Chem. Res.* **2008**, *41* (2), 157-167.
13. Shao, J. X.; Cheng, X. L.; Yang, X. D.; He, B., *Chinese Physics* **2006**, *15* (2), 329-333.
14. Luo, Y. R., *Handbook of Bond Dissociation Energies in Organic Compounds, New York: CRC Press* **2003**.
15. Volltrauer, H. N., *J. Hazard. Mater.* **1982**, *5* (4), 353-357.
16. Hiskey, M. A.; Brower, K. R.; Oxley, J. C., *J. Phys. Chem.* **1991**, *95* (10), 3955-3960.
17. Ng, W. L.; Field, J. E.; Hauser, H. M., *Journal of the Chemical Society-Perkin Transactions 2* **1976**, (6), 637-639.
18. Chakraborty, D.; Muller, R. P.; Dasgupta, S.; Goddard, W. A., *J. Phys. Chem. A* **2000**, *104* (11), 2261-2272.
19. Chakraborty, D.; Muller, R. P.; Dasgupta, S.; Goddard, W. A., *J. Phys. Chem. A* **2001**, *105* (8), 1302-1314.
20. Ng, W. L.; Field, J. E.; Hauser, H. M., *J. Appl. Phys.* **1986**, *59* (12), 3945-3952.
21. Pauling, L., *The Nature of the Chemical Bond, Cornell University Press* **1960**.
22. Murray, J. S.; Lane, P.; Nieder, A.; Klapotke, T. M.; Politzer, P., *Theor. Chem. Acc.* **2010**, *127* (4), 345-354.
23. de Bruin, T. J. M.; Lorant, F.; Toulhoat, H.; Goddard, W. A., *J. Phys. Chem. A* **2004**, *108* (46), 10302-10310.
24. Brook, A. G., *Acc. Chem. Res.* **1974**, *7* (3), 77-84.
25. Yu, Y. M.; Feng, S. Y., *J. Phys. Chem. A* **2004**, *108* (36), 7468-7472.

## Chapter 3

### FIRST-PRINCIPLES STUDY OF THE INITIAL DECOMPOSITION OF AZOBISTETRAZOLE AND AZOBISTRIAZOLE

#### Overview

Conventional C,N,O and H based energetic materials usually have NO<sub>3</sub> or NO<sub>2</sub> groups as the oxygen source and release energy by oxidizing C and H to form carbon dioxide, water and dinitrogen. Recently a new class of energetic material, nitrogen-rich compound, has gained considerable emphasis in the field of energetic material. Unlike conventional energetic materials, nitrogen-rich compounds release energy mainly by forming stable N<sub>2</sub>, as reflected on the fact that the bond energy per two-electron bond increases as the bond order between two nitrogen atoms goes from N–N (160 kJmol<sup>-1</sup>) and N=N (209 kJmol<sup>-1</sup>) to N≡N(318 kJmol<sup>-1</sup>, all normalized to one two-electron bond).<sup>1</sup> Pure single-bonded polymeric nitrogen solid has been regarded as the ultimate goal of nitrogen-rich compound. Such a polymeric solid has been found at pressure above 110GPa, but unfortunately decomposes to molecular nitrogen at 42GPa and room temperature.<sup>2</sup> Several N-rich molecular motifs, such as derivatives or salts of tetrazene<sup>3,4</sup>, tetrazole<sup>5-17</sup>, and triazole<sup>3,18-20</sup>, are proposed and synthesized, aiming to decrease their sensitivity and still retain the high heat of formation. A novel molecular motif, two tetrazole or triazole units connected by a azo(–N=N–) bridge, was found to be able to catenate up to 10 nitrogen atoms into a single molecule. Although with similar backbone structure, these materials have quite different sensitivities. Examples are 1,1'-azobistetrazole(**1**, extreme sensitive)<sup>7</sup>, 1,1'-azobis(5-methyltetrazole)(**2**, very sensitive)<sup>9</sup>, 2,2'-azobis(5-nitrotetrazole)(**4**, the most sensitive among the derivatives)<sup>21</sup>, 1,1'-azobis-1,2,3-triazole(**5**, sensitive)<sup>18</sup> and 4,4'-azo-1,2,4-triazole(**7**, stable)<sup>3</sup>, as reflected on their decomposition temperature and h<sub>50</sub> (see Table 1). The knowledge of the origin of sensitivity of energetic material at atomistic level is important because it provides guidance to intelligently design the new molecular motif

leading to energetic material with high heat of formation and low sensitivity. Sensitivity of energetic materials are known to correlate with many factors, such as the crystal orientation and morphology<sup>22, 23</sup>, hot spot formation<sup>24-26</sup>, bandgap<sup>27</sup>, and the distribution of electrostatic potential<sup>28, 29</sup>. Among these factors, the chemical property of material is the most direct and important one to determine the sensitivity of material. The ignition of energetic material is a positive feedback process, as heat released from the decomposition of one molecule triggers the decomposition of other cold molecules. There may exist many different reaction pathways, but the exothermic ones play more important roles in the initiation as they provide the energy necessary to propagate chain reactions. In this scenario, the barrier height it has to overcome to reach the first exothermic step is a key parameter to affect the sensitivity of energetic material. In this study, we used density functional theory (DFT) to calculate the unimolecular decomposition pathways for azobistetrazole and azobistriazole compounds, including three compounds (**3**, **6** and **8**) that have not been reported. We concluded that the barrier to the first exothermic step indeed highly correlates to the experimentally observed sensitivity, similar to the other highly sensitive material, Si-PETN.<sup>30</sup>

### **Computational methods**

All calculations were carried out with Jaguar 7.7 package, using the hybrid functional M06-2X to locate all the stationary points and calculate zero point energy and enthalpy at 6-311G\*\*++ basis set. All transition states (TS) were validated to have only one negative eigenvalue of the Hessian, followed by the minimum energy path (MEP) calculation to connect the reactant and product. Thermal dynamic data was taken at normal temperature and pressure. If not mentioned, enthalpies were reported.

### **Results and discussion**

The decomposition mechanism of compounds **1-8** and the enthalpy of intermediates were given in Figure 3-1 and 3-2. The theoretical heat of formation ( $\Delta H_{\text{formation}}$ ) and barrier height ( $\Delta H_{\text{barrier}}$ ) of

the rate-determining-step (RDS, marked in red in Figure 3-1) to the first exothermic reaction in these mechanisms were listed in Table 3-1, as well as experimental measured decomposition temperature and impact sensitivity of each compounds for comparison. The discussion proceeds by going through the decomposition mechanism of each compound.

**Table 3-1.** The theoretical heat of formation ( $\Delta H_{\text{formation}}$ ), barrier height ( $\Delta H_{\text{barrier}}$ ) and experimentally measured sensitivity of compounds **1-8**.

		Theoretical values in this work (kcal/mol)		Experimental results	
		$\Delta H_{\text{formation}}$	$\Delta H_{\text{barrier}}$	$T_{\text{decompose}}(^{\circ}\text{C})$	$H_{50}(\text{cm})$
1		251.1	28.9	80 <sup>7</sup>	<2 (<<1J) <sup>7</sup>
2		222.9	29.9	127.2 <sup>9</sup>	NA
3		246.2	33.1	NA	NA
4		277.9	34.2 <sup>a</sup>	Too sensitive to measure <sup>21</sup>	
5		213.6	43.5	193.8 <sup>18</sup>	16.6 <sup>18</sup>
6		204.4	60.5	NA	NA
7		190.3	55.0	313.36 <sup>19</sup>	55.9 (14.0J) <sup>19</sup>
8		173.1	54.9	NA	NA

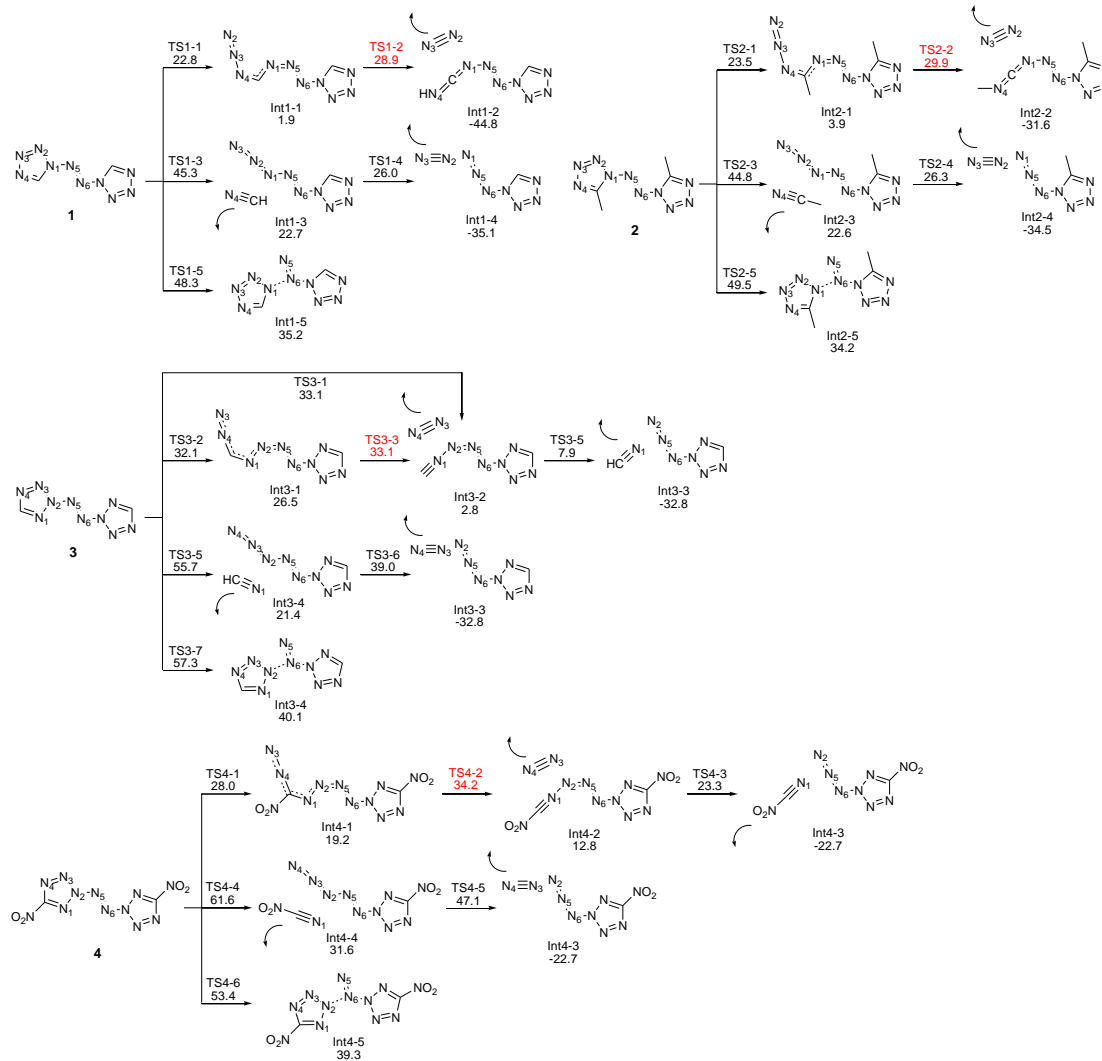


Figure 3-1. The decomposition mechanism of azobistetrazoles compounds **1-4**.

### 1. Azobistetrazoles:

1,1'-azobistetrazole (**1**) with ten N atoms catenated continuously in the molecule owns great sensitivity and decomposes at 80°C. We found that the easiest decomposition path starts with the N<sub>1</sub>-N<sub>2</sub> bond breaking to open the 5-member ring with a 22.8 kcal/mol barrier (TS1-1), as shown in Figure 3-1. The RDS is to dissociate N<sub>3</sub>-N<sub>4</sub> bond to release N<sub>2</sub> with a 28.9 kcal/mol barrier. After the TS1-2, the H on C shifts to the terminal N<sub>3</sub> to fulfill the valence and to form the final product, which is 44.8 kcal/mol more stable than **1**. This reaction has low barrier and high exothermicity and it may account for its high sensitivity. The other pathway is to strip HCN away from the

molecule via TS1-3, which has 45.3 kcal/mol barrier and we consider it less important for initiation, although the following reaction to release N<sub>2</sub> also has low barrier and high exothermicity. A simple N<sub>1</sub>-N<sub>5</sub> bond breaking results in TS1-5 and then the 5-member ring bounces back to form N<sub>1</sub>-N<sub>6</sub> bond (Int1-5), which is endothermic by 35.2 kcal/mol.

1,1'-azobis(5-methyltetrazole)(**2**) was experimentally found to be less sensitive than **1**, as reflected on its higher T<sub>decompose</sub>. We found its decomposition mechanism is similar with **1**. The corresponding barriers to open the 5-member ring (breaking N<sub>2</sub>-N<sub>3</sub>) and to release N<sub>2</sub> (breaking N<sub>3</sub>-N<sub>4</sub>) are both higher by 0.7 and 1.0 kcal/mol, which are consistent with experimentally measured lower sensitivity. The other exothermic reaction is to strip acetonitrile from **2** followed by N<sub>2</sub> releasing, which has higher overall barrier (44.8 kcal/mol) and is less important for the initiation.

2,2'-azobistetrazole (**3**) has not been reported experimentally. We found that it has similar heat of formation with **1** (246.2 vs. 251.1 kcal/mol), even the chain containing ten N atoms in the compound are branched. Similar ring-opening and N<sub>2</sub> releasing reactions are the exothermic reaction path with the lowest barrier (33.1 kcal/mol). This barrier is 4.2 kcal/mol higher than the one of **1**, hinting its higher stability of **3** and therefore may be more practical for real applications than **1**.

2,2'-azobis(5-nitrotetrazole)(**4**) is reported to be extremely sensitive and only very wet crystal can be handled in Ref 21. However after extensive search, the reaction mechanism is found to be similar with **3** and the overall barrier to the exothermic step is 34.2 kcal/mol, which is higher than the one of compounds **1**, **2** and **3**. This result does not agree with the extreme sensitivity observed experimentally in Ref 21. On the other hand, such a great sensitivity was not reported in the other reference,<sup>31</sup> which seems to agree with our theoretical result. Since the two experiments lead to big difference in sensitivity, we consider that the unexpected sensitivity of **4**, may result from one of the many other factors that can affect sensitivity for a given material. This includes the packing of the crystal, crystal morphology, impurities, or inclusion of solvent. In our current study we did not

examine the packing into a crystal and did not consider these other factors that might sensitize the compound 4 in Ref 21.

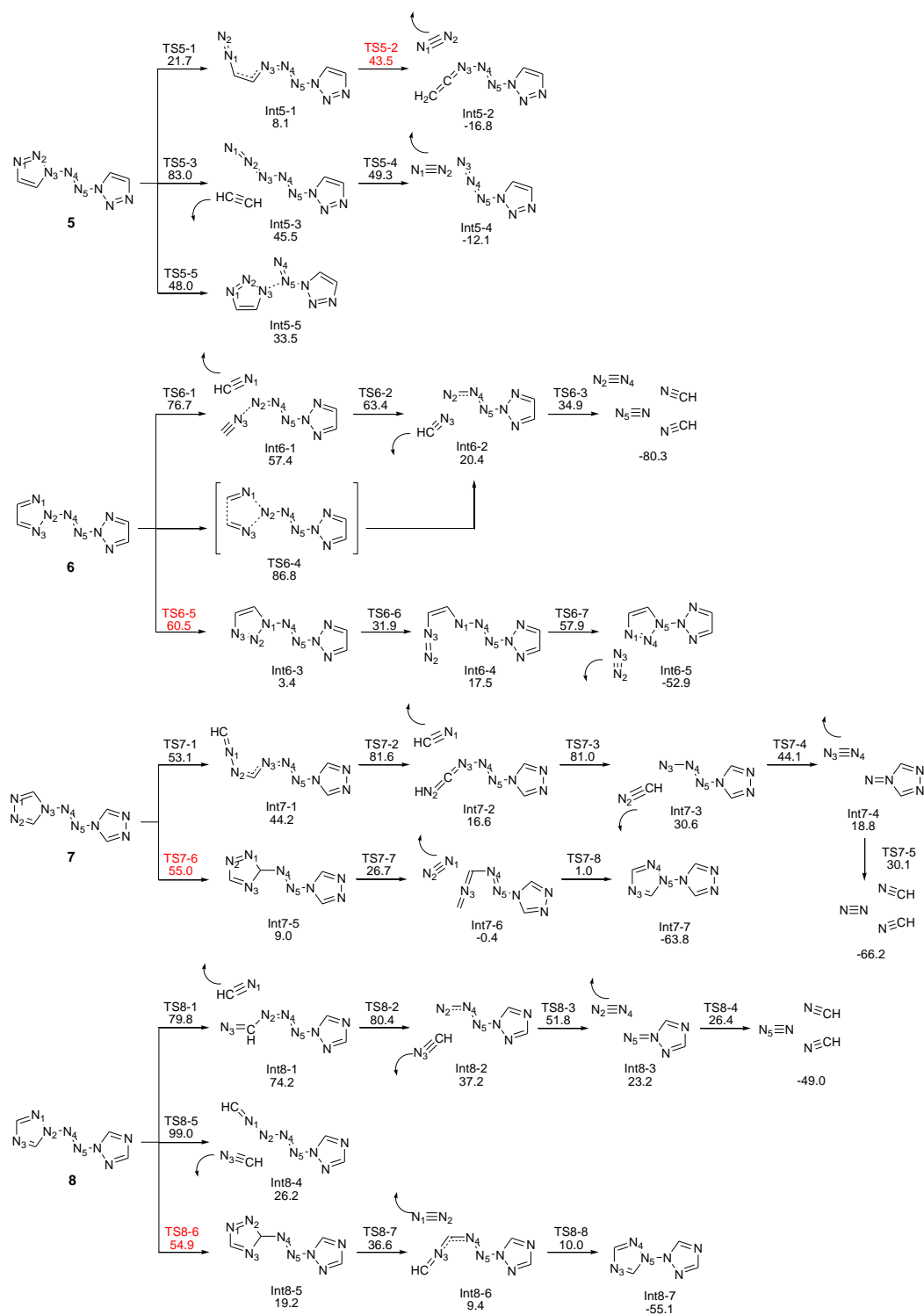


Figure 3-2. The decomposition mechanism of azobistriazoles compounds 5-8.

## 2. Azobistriazoles

In contrast to tetrazoles, triazoles have only three N atoms in the five-member ring and only some arrangements give N=N fragment that is easy to dissociate. For example, 1,1'-azobis-1,2,3-triazole (**5**) should be expected to have lower barrier for its clearly defined N=N fragments. The calculation showed that the decomposition of **5** starts with N<sub>2</sub>-N<sub>3</sub> bond breaking to open the five-member ring followed by cleaving C-N<sub>1</sub> bond to dissociate N<sub>2</sub> and heat releasing. The overall barrier of this mechanism is 43.5 kcal/mol, the lowest among azobistriazoles and agrees well with the experimental result that **5** is more sensitive than **7**. The other reaction to strip C<sub>2</sub>H<sub>2</sub> from **5** has high barrier (TS5-3, 83.0 Kcal/mol) and is highly endothermic (Int5-3, 45.5 kcal/mol) before the N<sub>2</sub> dissociating step, making it less important for initiation.

The valence bond structure of 2,2'-azobis-1,2,3-triazole (**6**) indicates the absence of N=N fragment. We found that the 5-member ring breaking pathway, the preferred pathway for **1-5**, has 76.7 kcal/mol barrier for **6**. The reason is that in compound **1-5**, this pathway leads to exothermic N<sub>2</sub> dissociation, whereas in compound **6**, the same pathway leads to HCN dissociation. HCN, although isolobal to N<sub>2</sub>, is quite energetic ( $\Delta H_{\text{formation}}=32.3 \text{ kcal/mol}^{32}$ ) so the step to dissociate HCN is generally endothermic. The other pathway to break the 5-member ring is to dissociate two HCN molecules simultaneously (TS6-4), which has 86.8 kcal/mol and it is the only concerted reaction to release two gas molecules found in this study. The exothermic reaction with the lowest barrier is via TS6-5 (60.5 kcal/mol), which breaks N<sub>2</sub>-N<sub>4</sub> bond and form N<sub>1</sub>-N<sub>4</sub> bond. This leads to the isomerization of one five-member ring of **6** so the N=N fragment can be stripped from the molecule, then the remaining backbone closes to form a new 1,2,3-triazole unit and releases heat.

4,4'-azo-1,2,4-triazole(**7**) has great stability, reflecting on its high decomposition temperature (313.36°C) and large H<sub>50</sub>(55.9cm). Theoretically, the stepwise HCN dissociations (TS7-1, TS7-2 and TS7-3) has the overall barrier 81.6 kcal/mol and only becomes exothermic to the very end of

reaction where N<sub>2</sub> is formed because of the high heat of formation of HCN. We found that the other exothermic reaction with lower barrier is via TS7-6 (55.0 kcal/mol), which breaks N<sub>3</sub>-N<sub>4</sub> bond and makes C-N<sub>4</sub> bond, leading to the isomerization of the 5-member ring with N=N fragment followed by N<sub>2</sub> dissociation (TS7-7) and the formation of 1,2,4-triazole (TS7-8), similar with the preferred mechanism found in **6**.

2,2'-azo-1,2,4-triazole(**8**) is an isomer of **7** and has not been reported experimentally. We found it contains less energy than **7**, as shown on its lower heat of formation (173.1 vs. 190.3 kcal/mol). The favored decomposition pathway is similar with **7**: first it breaks N<sub>2</sub>-N<sub>4</sub> bond and makes C-N<sub>4</sub> bond (TS8-6) to isomerize the 5-member ring to Int8-5, then N<sub>2</sub> dissociates from the 5-member ring (TS8-7) and the remaining backbone closes to form a new 1,2,4-triazole (Int8-7).

## Conclusion

Based on mechanisms above, we found the experimentally observed sensitivity highly correlates with the lowest barrier heights of highly exothermic reaction found in this study. The lower the barrier height, the higher the sensitivity, except compound **4**, for which the experimental results may not be conclusive.

Overall, with four N atoms in the five-member ring of azobistetrazaoles, a clearly-defined N=N fragment can always be found in the ring, and its decomposition starts with ring-opening to free one side of N=N followed by N<sub>2</sub> dissociation and heat generation. This barrier is around 28-35 kcal/mol for **1-4**, which is low enough to overwhelm other parameters and dominates the sensitivity of material. For azobistriazoles, only **5** has a N=N fragment in the original 5-member ring and similar ring-opening and N<sub>2</sub> dissociation pathway is favored. For **6**, **7** and **8**, an additional isomerization is necessary to release N<sub>2</sub>. This step breaks N-N bond and has the barrier around 55~60 kcal/mol, making these compound less sensitive.

## References

1. Klapötke, T. M., *Chemistry of High-energy Materials*. De Gruyter: 2011.
2. Eremets, M. I.; Gavriiliuk, A. G.; Trojan, I. A.; Dzivenko, D. A.; Boehler, R., *Nat. Mater.* **2004**, *3* (8), 558-563.
3. Li, S. H.; Pang, S. P.; Li, X. T.; Yu, Y. Z.; Zhao, X. Q., *Chin. Chem. Lett.* **2007**, *18* (10), 1176-1178.
4. Heppekausen, J.; Klapotke, T. M.; Sproll, S. A., *J. Org. Chem.* **2009**, *74* (6), 2460-2466.
5. Joo, Y. H.; Twamley, B.; Garg, S.; Shreeve, J. M., *Angew. Chem., Int. Ed.* **2008**, *47* (33), 6236-6239.
6. Klapoetke, T. M.; Sabate, C. M.; Rasp, M., *J. Mater. Chem.* **2009**, *19* (15), 2240-2252.
7. Klapotke, T. M.; Piercey, D. G., *Inorg. Chem.* **2011**, *50* (7), 2732-2734.
8. Klapotke, T. M.; Martin, F. A.; Stierstorfer, J., *Angew. Chem., Int. Ed.* **2011**, *50* (18), 4227-4229.
9. Tang, Y. X.; Yang, H. W.; Shen, J. H.; Wu, B.; Ju, X. H.; Lu, C. X.; Cheng, G. B., *New J. Chem.* **2012**, *36* (12), 2447-2450.
10. Fischer, D.; Klapotke, T. M.; Piercey, D. G.; Stierstorfer, J., *Chem.--Eur. J.* **2013**, *19* (14), 4602-4613.
11. Fischer, N.; Izsak, D.; Klapotke, T. M.; Stierstorfer, J., *Chem.--Eur. J.* **2013**, *19* (27), 8948-8957.
12. Hammerl, A.; Holl, G.; Klapotke, T. M.; Mayer, P.; Noth, H.; Piotrowski, H.; Warchhold, M., *Eur. J. Inorg. Chem.* **2002**, (4), 834-845.
13. Ye, C. F.; Xiao, J. C.; Twamley, B.; Shreeve, J. M., *Chem. Commun.* **2005**, (21), 2750-2752.
14. Klapoetke, T. M.; Sabate, C. M., *Chem. Mater.* **2008**, *20* (5), 1750-1763.
15. Klapoetke, T. M.; Sabate, C. M., *New J. Chem.* **2009**, *33* (7), 1605-1617.
16. Klapotke, T. M.; Piercey, D. G.; Stierstorfer, J., *Chem.--Eur. J.* **2011**, *17* (46), 13068-13077.

17. Fischer, N.; Huell, K.; Klapoetke, T. M.; Stierstorfer, J.; Laus, G.; Hummel, M.; Froschauer, C.; Wurst, K.; Schottenberger, H., *Dalton Trans.* **2012**, 41 (36), 11201-11211.
18. Li, Y. C.; Qi, C.; Li, S. H.; Zhang, H. J.; Sun, C. H.; Yu, Y. Z.; Pang, S. P., *J. Am. Chem. Soc.* **2010**, 132 (35), 12172-12173.
19. Qi, C.; Li, S. H.; Li, Y. C.; Wang, Y. A.; Chen, X. K.; Pang, S. P., *J. Mater. Chem.* **2011**, 21 (9), 3221-3225.
20. Huang, Y.; Gao, H.; Twamley, B.; Shreeve, J. n. M., *Eur. J. Inorg. Chem.* **2008**, (16), 2560-2568.
21. Klapoetke, T. M.; Piercey, D. G.; Stierstorfer, J., *Dalton Trans.* **2012**, 41 (31), 9451-9459.
22. Dick, J. J.; Mulford, R. N.; Spencer, W. J.; Pettit, D. R.; Garcia, E.; Shaw, D. C., *J. Appl. Phys.* **1991**, 70 (7), 3572-3587.
23. Czerski, H.; Proud, W. G., *J. Appl. Phys.* **2007**, 102 (11), 8.
24. Field, J. E.; Bourne, N. K.; Palmer, S. J. P.; Walley, S. M.; Smallwood, J. M., *Philosophical Transactions of the Royal Society of London Series a-Mathematical Physical and Engineering Sciences* **1992**, 339 (1654), 269-283.
25. Tokmakoff, A.; Fayer, M. D.; Dlott, D. D., *J. Phys. Chem.* **1993**, 97 (9), 1901-1913.
26. Cai, Y.; Zhao, F. P.; An, Q.; Wu, H. A.; Goddard, W. A.; Luo, S. N., *J. Chem. Phys.* **2013**, 139 (16), 164704.
27. Zhu, W.; Xiao, H., *Struct. Chem.* **2010**, 21 (3), 657-665.
28. Murray, J. S.; Lane, P.; Politzer, P.; Bolduc, P. R., *Chem. Phys. Lett.* **1990**, 168 (2), 135-139.
29. Murray, J. S.; Lane, P.; Politzer, P., *Mol. Phys.* **1995**, 85 (1), 1-8.
30. Liu, W. G.; Zybin, S. V.; Dasgupta, S.; Klapoetke, T. M.; Goddard, W. A., *J. Am. Chem. Soc.* **2009**, 131 (22), 7490-7491.

31. Bottaro, J. C.; Penwell, P. E.; Schmitt, R. J. N,N'-azobis-nitroazoles and analogs thereof as igniter compounds for use in energetic compositions. US 5889161 A, 1999.
32. NIST Chemistry WebBook.

## Chapter 4

### FIRST PRINCIPLES STUDY OF IGNITION MECHANISM OF HYPERGOLIC BIPROPELLANT: N,N,N',N'-TETRAMETHYLETHYLENEDIAMINE (TMEDA), N,N,N',N'-TETRAMETHYLMETHYLENEDIAMINE (TMMDA) AND NITRIC ACID

#### Overview

Hypergolic bipropellants are fuel oxidizer pairs that ignite spontaneously upon mixing. Such propellants are useful for space propulsion because they can be fired any number of times by simply opening and closing the propellant valves until the propellants are exhausted. Common hyperbolic propellant combinations include nitrogen tetroxide (NTO)/monomethylhydrazine (MMH, MeHN-NH<sub>2</sub>)<sup>1, 2</sup> and NTO/unsymmetrical dimethyl hydrazine (UDMH, Me<sub>2</sub>N-NH<sub>2</sub>)<sup>3, 4</sup>. However the carcinogenicity and toxicity of hydrazine derivatives makes it important to seek new low-toxicity hypergolic fuels<sup>5</sup>. Alkyl multiamines have been suggested as candidates to replace toxic hydrazine derivatives and experiments aimed at selecting the optimum saturated tertiary alkyl multiamines have been reported<sup>6</sup>.

A common screen for the reactivity of bipropellants is the drop-test, which involves dropping fuel into the pool of oxidizer or vice versa. The *ignition delay*, defined as the time interval from the touch of two liquid surfaces to the appearance of a flame, is an indicator of reactivity. Among various

alkylamines, N,N,N',N'-tetramethylethylenediamine (TMEDA) (Figure 4-1a) is considered as promising because of its short ignition delay<sup>7</sup> (14 ms) when reacting with white fuming nitric acid

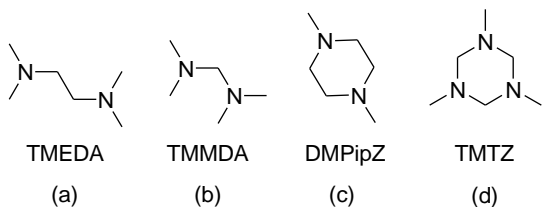


**Figure 4-1.** Structures of several alkyl amines (a) TMEDA (b) TMMDA (c) DMPipZ, (d) TMTZ

(WFNA), which consists of pure  $\text{HNO}_3$  (no more than 2% water and less than 0.5% dissolved nitrogen dioxide or dinitrogen tetroxide). In contrast, N,N,N',N'-tetramethylmethylenediamine (TMMDA), a similar diamine linked by a single  $\text{CH}_2$  group rather than two (Figure 4-1b) exhibits significantly longer ignition delay<sup>8</sup> (30ms) when reacting with white fuming nitric acid (WFNA). A similar dependence of ignition delay on the linker length is also observed in the drop-test of 1,4-dimethylpiperazine (DMPipZ, Figure 4-1c, 10ms ignition delay) with two linkers between the amines each with two  $\text{CH}_2$  groups whereas 1,3,5-trimethylhexahydro-1,3,5-triazine (TMTZ, Figure 4-1d), with one  $\text{CH}_2$  group is not hypergolic under the same experimental condition. The above results can be summarized as: *diamines linked by two  $\text{CH}_2$  groups have much shorter ignition delay than those linked by a single  $\text{CH}_2$ .* Thus, even though ignition delay is a macroscopic measurement involving complex chemical and physical factors such as diffusion and thermal conduction, we find an atomistic level mechanism that explains the macroscopic phenomenon.

Based on the above observation and QM calculations (PBE flavor of DFT), McQuaid suggested a correlation between the ignition delay and the angle between orientations of the lone pair on nitrogen and the N-C/C-C bond<sup>9</sup>. Later, a QM mechanistic study (at G3MP2 level) of the early reaction between TMEDA and  $\text{NO}_2$  was reported, in which an intermediate with C-C double bond was formed from the nitrite or nitro intermediate with both barriers higher than 23 kcal/mol<sup>10</sup>. The reaction mechanism of TMMDA and  $\text{NO}_2$  has not previously been studied and no mechanism has yet explained why a  $\text{CH}_2\text{-CH}_2$  linker between two amines leads to shorter ignition delay than for a single  $\text{CH}_2$  group.

Wang et al.<sup>7</sup> proposed that the reaction between TMEDA and  $\text{HNO}_3$  starts with an exothermic salt formation, in which the proton transfers from each of two  $\text{HNO}_3$  molecules to each of the two nitrogen atoms on TMEDA to form the salt of alkyl diaminium and dinitrate anion (TMEDADN). The heat

released from the salt formation raises the local temperature at the interface between two liquids, leading to decomposition of  $\text{HNO}_3$  into  $\text{NO}_2$ ,  $\text{O}_2$  and  $\text{H}_2\text{O}$ , followed by  $\text{NO}_2$  reacting with TMEDA to form various free radicals and HONO, which is observed in the IR spectra in the gas product. The remaining free radicals would undergo further reaction, such as free radical recombination with  $\text{NO}_2$  or breaking into smaller fragments, heating up the mixture and initiating more chain reactions. In this salt formation mechanism, two important factors have a major influence on the ignition delay:

- (1) the exothermicity of the salt formation, and
- (2) the rate of fuel molecules reacting with  $\text{NO}_2$ .

To investigate how the linker length affects these two factors, we considered the following questions:

1. How much energy is released when the nitrate salts of TMEDA and TMMDA are formed at the interface between two liquid surfaces?
2. What is the mechanism for TMEDA and TMMDA reacting with  $\text{NO}_2$ ?

To approach the first question, we used the density functional theory (DFT) method with the B3LYP functional to calculate the energy release of TMEDA and TMMDA reacting with two  $\text{HNO}_3$  molecules to form dinitrate salt using a dielectric cavity to model the solvent effect. The experimental measurement of ignition delay involves dropping the fuel into the pool of nitric acid. Therefore our calculations used solvent parameters taken from pure nitric acid to approximate the complex interface between the two liquid surfaces.

To answer the second question, we calculated all bond energies in TMEDA and TMMDA and compared with the bond energies for their alkane analogues to see how the presence of nitrogen atoms affects the bond energies. Furthermore, we carried out a mechanistic study on the system of TMEDA/ $\text{NO}_2$  and TMMDA/ $\text{NO}_2$  in gas phase at the same level of theory, calculating the potential energy surface and reaction pathway to determine how the reaction is initiated and how the connecting alkyl group can affect the reaction. We also studied the initiation reaction of TMEDADN/ $\text{NO}_2$  and

the dinitrate salt of TMMDA (TMMDADN)/NO<sub>2</sub> in gas phase to determine how the salt formation changes the reactivity of such fuels.

### **Computational methods**

All calculations were carried out with Jaguar 7.5 package, using the unrestricted hybrid functional UB3LYP to locate all stationary points and to calculate zero point energy and enthalpy using the 6-311G\*\* basis set. All transition states (TS) were validated to have exactly one negative eigenvalue of the Hessian followed by the minimum energy path (MEP) scan to connect reactant and product. Thermodynamic data was evaluated at 298.15 K and 1 atm. Solvation effect was calculated using the Poisson-Boltzmann (PB) method as implemented in Jaguar, using the experimental dielectric constant ( $\epsilon=50$ ) and solvent radius ( $R_{\text{nitric acid}}=2.02\text{\AA}$ ) for pure nitric acid<sup>11</sup>.

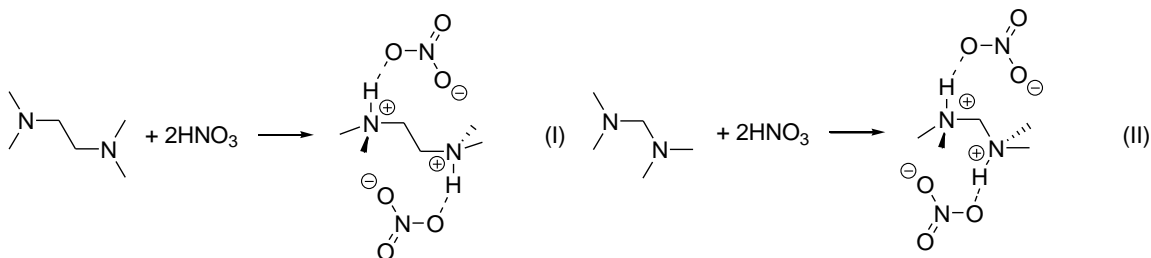
### **Results and discussion**

The results are presented in the following manner. In Section 1 the heat of salt formation of both TMEDA and TMMDA are presented, with various bond energies in TMEDA, TMMDA and their alkane analogues in Section 2. Section 3 contains reaction mechanism for TMEDA reacting with NO<sub>2</sub> and Section 4 contains the mechanism of TMMDA reacting with NO<sub>2</sub>. Section 5 compares how the molecular structure of TMEDA and TMMDA affects the reaction mechanisms. Section 6 compares the initiation for NO<sub>2</sub> reacting with these two diamines and their dinitrate salts, TMEDADN and TMMDADN.

#### **1. Exothermicity of the formation of dinitrate salt of TMEDA and TMMDA**

Upon dropping TMEDA into a pool of HNO<sub>3</sub>, condensed-phase TMEDA dinitrate is observed (using a high-speed camera) as a white cloud forming along the surface of the

contacting liquids<sup>7</sup>. In this reaction protons from HNO<sub>3</sub> are transferred to the N lone pairs on TMEDA and TMDMA as illustrated in (I) and (II).



For TMEDADN, N-H distance is 1.058Å and O-H distance is 1.647Å while for TMMDADN, N-H distance is 1.062Å and O-H distance is 1.639Å. These short N-H bonds show that the protons are fully transferred to the N atoms to form a di-cation di-anion pair.

For reaction (I) to form TMEDADN, the total solution phase energy, which includes the QM electronic energy and the PB interaction of the molecule with the dielectric solvent cavity, is exothermic by 45.0 kcal/mol. For reaction (II), to form TMMDADN this reaction is downhill by 38.7 kcal/mol, which is 6.3 kcal/mol less exothermic than the formation of TMEDADN. The smaller energy release results from the shorter distance between two positive charged N atoms in TMMDADN (2.518Å) compared to 3.838Å in TMEDADN, leading to a larger electrostatic repulsion for the doubly protonation. The decreased exothermicity from forming TMMDADN should lead to a lower local temperature, contributing to the longer ignition delay of the reaction between TMDMA and HNO<sub>3</sub>.

## 2. Bond energies in TMEDA, TMDMA and their alkane analogues

Although it is the barrier height that determines the reaction rate, one can often estimate the relative barriers from the changes in the bond energies, providing a hint about chemical reactivity.

The gas-phase bond energies in TMEDA, TMMDA and their alkane analogues, 2,5-dimethylhexane and 2,5-dimethylpentane are listed in Table 4-1. Particular points to note:

- The C<sup>1</sup>-N<sup>2</sup> bonds in TMEDA and TMMDA are 7 to 10 kcal/mol weaker than the corresponding C-C bonds.
- The C-H bonds in TMEDA and TMMDA are 10 kcal/mol weaker than C-H bonds in the alkane.
- The C-C bond in TMEDA is significantly weaker by 18 kcal/mol than the corresponding C-C bond in its alkane analogue.

Thus the C<sup>1</sup>-H bond energies in TMEDA and TMMDA are 86.3 and 86.4 kcal/mol, compared with the C-H bond energy in their alkane analogues, 96.6 and 96.2 kcal/mol. Similar reductions in bond energy are also found for C<sup>3</sup>-H bonds. This is because after breaking the C-H bond, the free radical on C increases the strength of the C<sup>3</sup>-N bond by ~10 kcal/mol due to the interaction with the lone pair electrons on N (a three-electron-two-center bond). This extra bonding between C and N stabilizes the final product and lowers the C-H bond energies. Such extra bonding can take place only if the free radical is adjacent to atoms having lone pairs.

By the same stabilization effect, the C<sup>3</sup>-N<sup>2</sup> bond in TMMDA is weaker than the corresponding C<sup>3</sup>-N<sup>2</sup> bond in TMEDA by 3 kcal/mol, and the drastically lower C<sup>3</sup>-C<sup>4</sup> bond energy for TMEDA is due

**Table 4-1.** Bond energies in TMEDA, TMMDA, and their corresponding alkane analogues from B3LYP calculations

Bond Energies (kcal/mol)	TMEDA	2,5-dimethylhexane	TMMDA	2,5-dimethylpentane
C <sup>1</sup> -H	86.3	96.6	86.4	96.2
C <sup>1</sup> -N <sup>2</sup> /C <sup>2</sup>	68.3	79.6	71.7	78.4
C <sup>3</sup> -N <sup>2</sup> /C <sup>2</sup>	66.9	75.0	63.1	75.4
C <sup>3</sup> -H	84.5	91.6	85.2	92.3
C <sup>3</sup> -C <sup>4</sup>	60.5	78.9	-	-

to the stabilization on both dissociation products. This makes this C-C bond the weakest bond in TMEDA, which is responsible for the fundamental difference in reactivity between TMEDA and TMMDA drastically lower than the one in its alkane analogue by 18 kcal/mol due to the stabilization on both dissociation products, rendering this C-C bond the weakest bond in TMEDA, which leads to the fundamental difference in reactivity between TMEDA and TMMDA.

### 3. Reaction mechanism of TMEDA+NO<sub>2</sub>

The various stages of the reactions in gas phase between TMEDA and NO<sub>2</sub> are shown in Scheme 1, which can be categorized into 6 types:

1. H-abstraction by NO<sub>2</sub> to form HONO while leaving a free radical on C. (reactions to INT1, INT2, INT11 and INT12)
2. Trapping by NO<sub>2</sub> of the free radical formed by H-abstraction (leading to INT4, INT5, INT6 and INT8).
3. C-C double bond formation upon extraction of an H by NO<sub>2</sub>, (leading to INT7) followed by reactions with NO<sub>2</sub> to form INT11 and INT12.
4. Rearrangement of INT4 and INT8 to break C-N bonds (leading to INT9, INT10, and INT13).
5. C-C bond breaking events: the C-C bond can be broken by simultaneous attack of two NO<sub>2</sub> on TMEDA (forming INT3), by the rearrangement of INT8 to form INT14 or INT15, or by the rearrangement of INT11 through a 4-member ring intermediate (INT16 or INT17) to form INT18.
6. Epoxide formation (INT19).

Figure 4-2 includes the enthalpy (no parentheses) and Gibbs free energy at 298.15K (in parentheses) of each species from the QM calculations, using the energies of separated TMEDA and NO<sub>2</sub> in the gas phase as the reference.

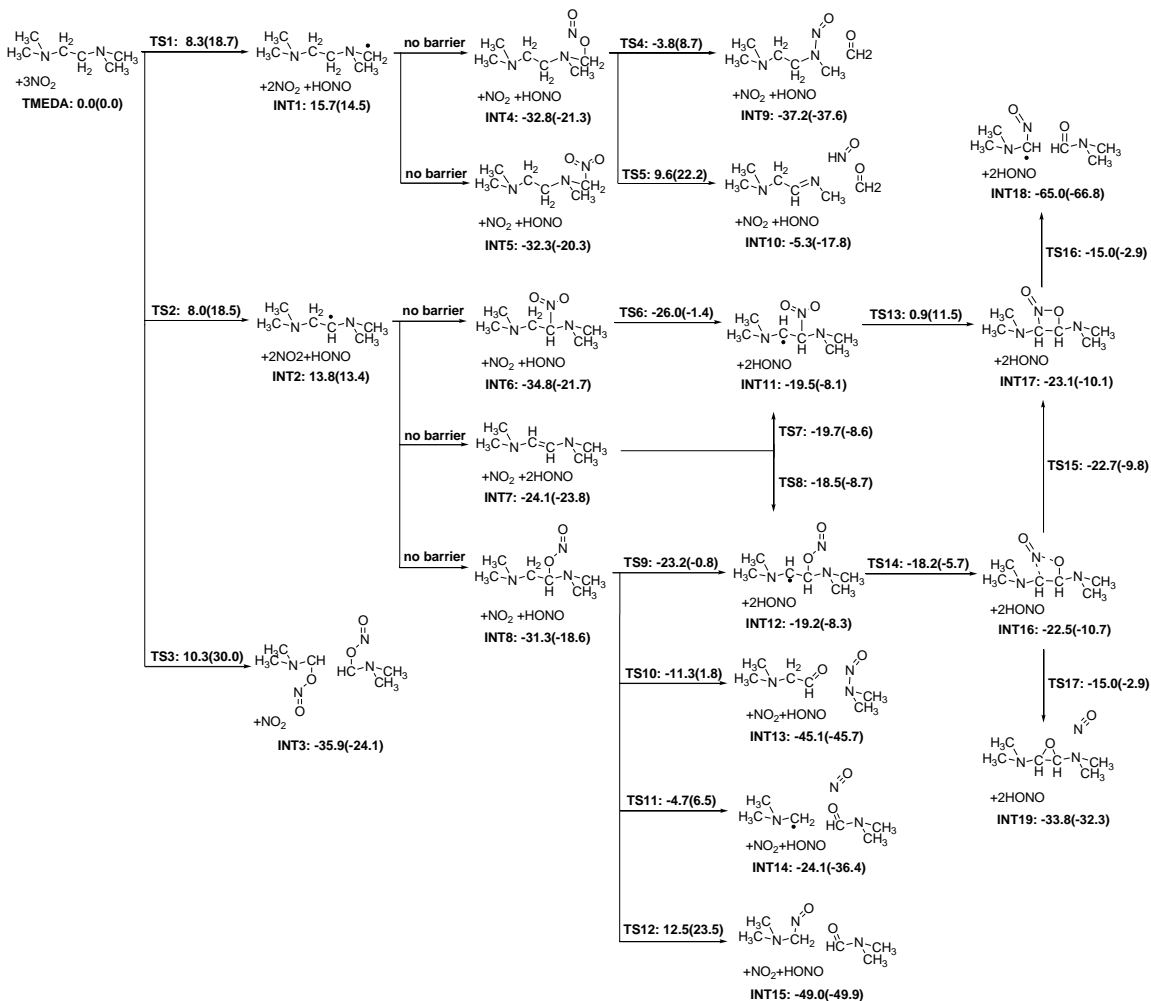


**Figure 4-2.** Reactions between TMEDA and  $\text{NO}_2$ . Enthalpy and Gibbs free energy at 298.15K (in parentheses) of each species are provided in kcal/mol.

### 3.1. Initiating stage

Based on MMH/NTO mechanism<sup>12</sup>, where the HONO formation happens first, the reaction between TMEDA and  $\text{NO}_2$  can be initiated with  $\text{NO}_2$  abstracting the hydrogen on the terminal methyl group (TS1, Figure 4-3a) or the middle ethyl group (TS2, Figure 4-3b). There are three possible conformations for  $\text{NO}_2$  abstracting H with different  $\text{NO}_2$  orientation: 1. *cis*-HONO formation, 2. *trans*-HONO formation, 3.  $\text{HNO}_2$  formation. We determined the barriers for various TS geometries and found that formation of *cis*-HONO is always the lowest, followed by the  $\text{HNO}_2$  (higher by about 3

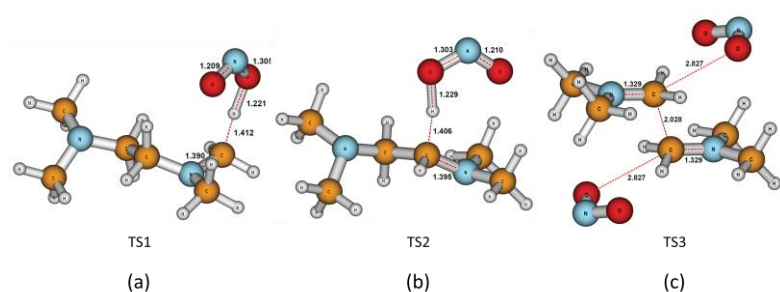


**Figure 4-3.** Structures of (a)TS1 (b)TS2 (c)TS3

kcal/mol) and then *trans*-HONO formation (higher by 7-8 kcal/mol), so only the TS for *cis*-HONO formation is reported here. The lower barrier for *cis*-HONO formation arises because of the improved interaction between the C-H bond and the  $A^1$  radical orbital on  $\text{NO}_2$  (in plane with the higher amplitude on the oxygens, same phase<sup>13</sup>). For *trans*-HONO formation, the TS has the distance of the H from the second O about 1 Å longer than the one in *cis* conformation, resulting in a smaller interaction between free-radical orbital and C-H bond, hence the higher barrier. The trend found here that *cis*-HONO is favored differs from the trend of the HONO formation in MMH/ $\text{NO}_2$  system<sup>14</sup>, which has multiple polar N-H bonds allowing *trans*-HONO to interact with both the breaking N-H bond via the O atom and the adjacent N-H bond through the N atom on  $\text{NO}_2$ , lowering the barrier. The barrier for  $\text{NO}_2$  to abstract H on the linker ethyl group is 8.0 kcal/mol, essentially the same as the 8.3 kcal/mol to abstract H from the terminal methyl group. The increased entropy for bringing these two gas phase molecules together at the TS raises the Gibbs free energy by about 10 kcal/mol for both reactions. To separate the product complex of HONO and TMEDA free radical to form intermediates INT1 and INT2 requires another 7~8 kcal/mol. Comparing with TMEDA, the barriers of HONO formation from 2,5-dimethyl-hexane are about 10 kcal/mol higher, indicating that the N atom adjacent to the C-H bond both reduces the C-H bond energy as shown before and also lowers the barrier for HONO abstraction. At the TS, the nitrogen donates its lone pair electrons to the antibonding C-H orbital, stabilizing the TS and lowering the barrier.

Besides the two HONO formation pathways to form INT1 and INT2, we found that simultaneous attack of two  $\text{NO}_2$  to both ends of the relative weak C-C bond (TS3, Figure 4-3c), breaks the C-C

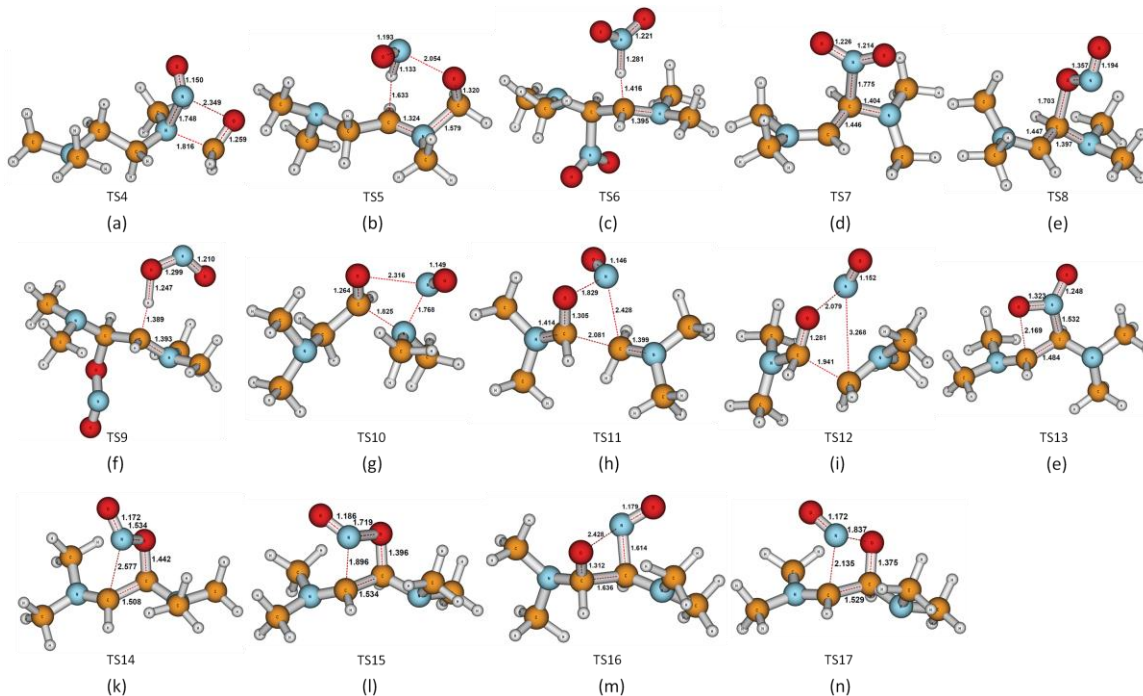


**Figure 4-4.** Structures of (a)TS4 (b)TS5 (c)TS6 (d)TS7 (e)TS8 (f)TS9 (g)TS10 (h)TS11 (i)TS12 (j)TS13 (k)TS14 (l)TS15 (m)TS16 (n)TS17

bond to form two  $\text{ONO-CH}_2\text{N}(\text{CH}_3)_2$  fragments. This path leads to an unusually low enthalpy barrier (10.3 kcal/mol) for C-C bond breaking because that the lone pair electrons of both N atoms donate into the C-C antibonding orbital from both ends. This stabilizes both free radicals formed upon C-C bond dissociation as shown before. However this requires a termolecule-reaction, leading to an entropy decrease that raises the free energy at the TS to 30.0 kcal/mol, making this pathway unlikely in the gas phase. On the other hand, for the condensed mixture of TMEDA and  $\text{HNO}_3$ , where  $\text{NO}_2$  molecule is the solute, this entropy cost will decrease, reducing the free energy barrier to make this pathway more viable.

### 3.2 Reactions after INT 1

After H-abstraction, the TMEDA free radical on the terminal methyl group, INT1, can recombine with other  $\text{NO}_2$  radicals. The recombinations to form INT4 and INT5 are about 46 kcal/mol exothermic with no barriers. From INT4, it is quite favorable to eliminate the NO, leaving an O

radical on the fragment. This O radical can then form a C-O double bond while breaking the C-N bond, leaving a bimolecular-like state, of formaldehyde molecule plus an N radical. The dissociating NO can either recombine with N radical (TS4, Figure 4-4a) to form INT9 with a barrier 29.0 kcal/mol, or abstract one H from C (TS5, Figure 4-4b) to form a C-N double bond and HNO molecule (INT10) but with a much higher barrier, 42.5 kcal/mol. The nitro compound INT5 is less reactive and may play a small role at the initial stage when temperature is low.

### 3.3 Reactions after INT2

Similar to INT1, the free radical on the middle ethyl of TMEDA, INT2, can recombine with another NO<sub>2</sub> free radical to form nitro and nitrite compounds, INT6 and INT8, without a barrier while releasing more than 45 kcal/mol of energy. INT6 and INT8 can lose H again through HONO formation via TS6 (Figure 4-4c) and TS9 (Figure 4-4f) to form free radical intermediate INT11 and INT12 with barriers about 8kcal/mol, similar to barriers to lose the first H.

In addition to recombination, NO<sub>2</sub> can also abstract H on the carbon next to the radical site to form a C-C double bond (INT7), which is also barrierless and exothermic by 37.9 kcal/mol. These three reactions are very exothermic and non-reversible. Consequently, their relative reaction rates to form INT6, INT7 and INT8 may be dominated by the kinetics of interactions with the NO<sub>2</sub>, rather than the thermodynamics of products formation.

The NO<sub>2</sub> can open the double bond in INT7, converting to INT11 via TS7 (Figure 4-4d), and INT12 via TS8 (Figure 4-4e). The TS we located for opening double bond (TS8) to form INT12, has a lower energy than INT12 after including the zero point energy (ZPE),

suggesting that INT12 is not be a stable intermediate in gas phase, but it may play a role in the condensed phase.

The formation of INT7 containing the C-C double bond is important because this double bond is fairly easily to oxidize in acid (compared with the saturated bonds). Some possible low barrier mechanisms for C-C and C-N bond breaking are proposed and discussed below.

Like INT4, INT8 can decompose unimolecularly to eliminate NO from the -ONO group.

The subsequent formation of the C-O double bond can lead to:

1. C-N bond breaking and N-N bond formation (via TS10, Figure 4-4g) to form INT13. Indeed the ON-N(CH<sub>3</sub>)<sub>2</sub> moiety has been identified in the IR spectrum of the gas product of TMEDA and HNO<sub>3</sub><sup>7</sup>.
2. C-C bond breaking (via TS11 and TS12, see Figure 4-4h and i). TS11 is 17.2 kcal/mol lower than TS12 due to the less strained geometry, despite the new C-N bond and greater exothermicity of the product from TS12. Although INT14 and INT10 are similar, TS10 is 7.5 kcal/mol lower than TS5 because the formaldehyde C-O double bond is weaker than the primary aldehyde bond in INT14.

Comparing with the above unimolecular reactions (involving favorable entropic effects), the H-abstraction by NO<sub>2</sub> has the lowest enthalpic barrier (8.1) and free energy barrier (17.8 kcal/mol) (TS9, Figure 4-4f). The product free radical can react with the O in the -ONO group to form an epoxide (INT19) and NO via TS17 (Figure 4-4h), or it can react with the N to form a 4-member ring intermediate, INT17, with negligible barrier (< 2 kcal/mol). With the help of lone pairs on N atoms, breaking the C-C bond in the 4-member ring intermediate has a barrier of only 8.1 kcal/mol. This ring breaking reaction starts with N-O bond breaking,

followed by C-O double bond formation, leading to C-C bond fission (TS16, Figure 4-4m) to release 41.9 kcal/mol. In addition to the considerable exothermicity, this reaction produces two reactive fragments, an amino aldehyde and a free radical, that can induce further reactions. The amino aldehyde products is stable and has been observed via IR spectroscopy<sup>7</sup> as a gas product of the reaction between TMEDA and HNO<sub>3</sub>. This differs from the free radical recombination, which reduces the number of reactive molecules and is entropically unfavorable.

#### **4. Reaction mechanism of TMMDA+NO<sub>2</sub>**

The reactions of TMMDA with NO<sub>2</sub> are similar to those between TMEDA and NO<sub>2</sub>, except there is no C-C double bond formation and C-C bond breaking. Three types of reactions are:

1. H abstraction by NO<sub>2</sub> (reactions to INT20 and INT21) leaving a free radical on TMMDA.
2. Free radical recombination of NO<sub>2</sub> with the product from H abstraction (reactions to INT22, INT23, INT24 and INT25).
3. Breaking the C-N bond on TMMDA to form a new N-N bond (reactions to INT26 and INT28) or a C-N double bond (reaction to INT27).

The enthalpy and Gibbs free energy of each species is marked in Figure 4-5 and referenced to the sum of individual TMMDA and NO<sub>2</sub> energies in the gas phase.

##### **4.1. Initiating stage: H-abstraction.**

The reaction starts with NO<sub>2</sub> abstracting H on the terminal methyl groups (via TS18, Figure 4-6a, to INT20) or the middle -CH<sub>2</sub>- group (via TS19, see Figure 4-6b to INT21) to form HONO. All barriers are very similar to those of TMEDA. Although the lone-pair electron on nitrogen can stabilize the TS for H-abstraction, as seen for TMEDA, abstracting the H from the middle methyl group between two nitrogen atoms does not get a double effect because the lone-pairs on neighboring nitrogen atoms orient perpendicular to each other due to steric repulsion so that only one lone-pair has the right orientation to donate electron into the antibonding orbital of C-H bond to stabilize the transition state. As a result, the barrier height of 8.8kcal/mol is similar to same reactions in TMEDA.

#### 4.2. Reactions after INT20

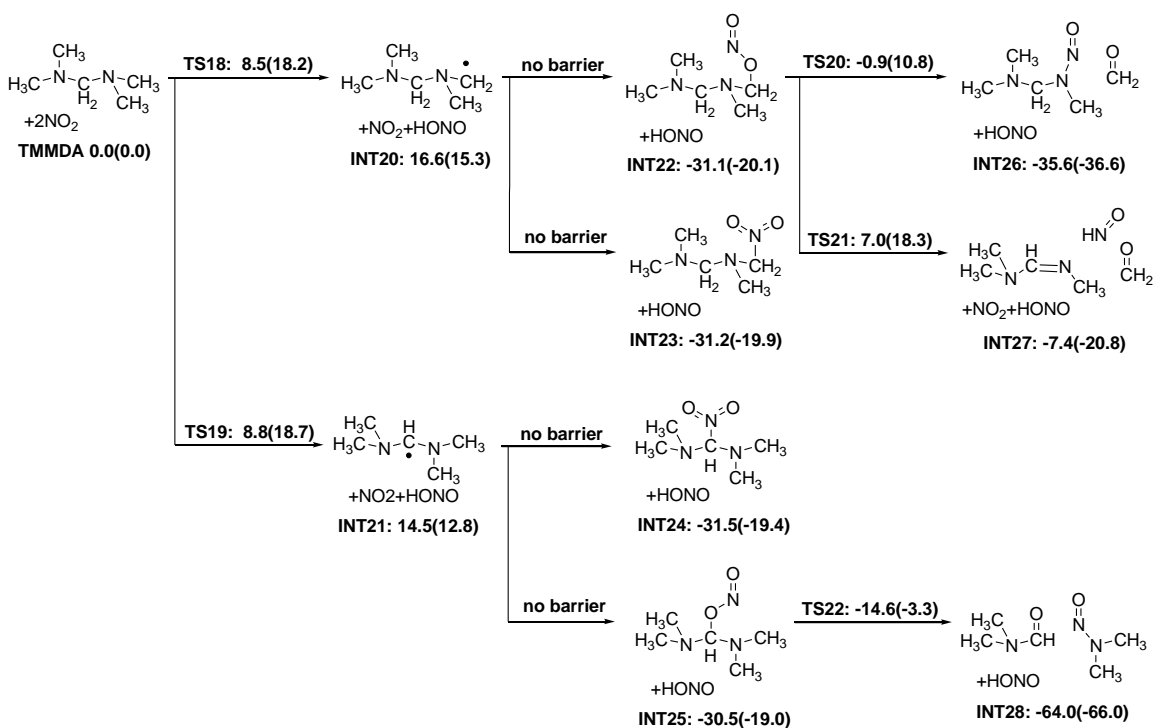


**Figure 4-5** Reactions between TMMDA and NO<sub>2</sub>. Enthalpy and Gibbs free energy (in parentheses) of each species are provided in kcal/mol.

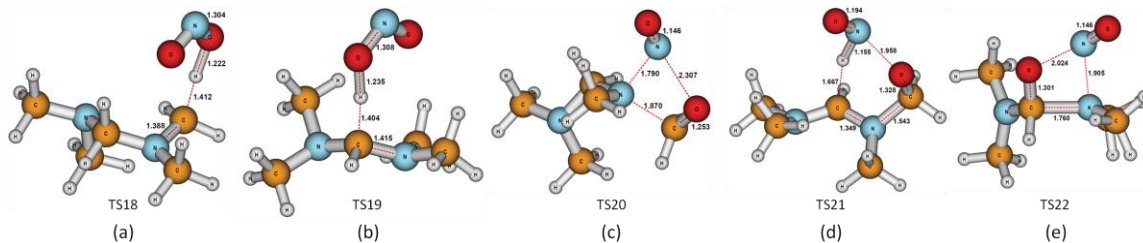


**Figure 4-6.** Structures of (a)TS18 (b)TS19 (c)TS20 (d)TS21 (e)TS22

Without the possibility of forming a C-C double bond, the only favorable pathway to oxidize TMMDA is via free radical recombination to generate nitro or nitrite compounds (INT22, INT23, INT24 and INT25). All reactions are exothermic by 30 to 31 kcal/mol. The nitrite compound can undergo unimolecular reaction to break the C-N bond while forming the C-O double bond to generate formaldehyde, followed by forming a N-N bond (via TS20, Figure 4-6c, to INT26) or a C-N double bond (via TS21, Figure 4-6d, INT27), which are similar to reactions to INT9 and INT10 in Figure 4-2.

The same C-N bond breaking and C-O double bond formation can also take place on INT25 via TS22 (Figure 4-6e), generating an amino aldehyde and a N-nitroso fragment with a 15.9 kcal/mol barrier, releasing considerable energy, 33.5 kcal/mol. This path also generates two reactive fragments that can each be further oxidized easily.

## 5. Comparison between reaction mechanisms of TMEDA/NTO and TMMDA/NTO

In both systems, the initiation reaction is HONO formation, which is also observed experimentally in hydrazine derivative/NTO<sup>12, 15</sup> and NH<sub>3</sub>/NTO<sup>16</sup> systems. This step has a low barrier but is endothermic, making it not helpful for initiating other reactions that might have higher barriers. The exothermic steps usually involve the oxidation of C, such as free radical recombination (forming a new C-N or C-O bond) or C-O double bond formation. The barrier to oxidize carbon via a free radical recombination pathway is similar for both TMEDA and TMMDA, since these

free radicals are generated by HONO formation, which has barrier around 8-9 kcal/mol for both fuels. However, C oxidation via C-O double bond formation has quite different barriers for TMEDA and TMMDA. In TMMDA, the most favorable pathway to form the C-O double bond is from INT25 to INT28, which has a barrier 15.9 kcal/mol. In contrast, for TMEDA, this can occur via several pathways. Starting from intermediate INT7 with a C-C double bond, the highest barrier on the pathway to reach the product with a C-O double bond, INT18, is 8.1 kcal/mol (at TS16). This lower barrier for C oxidation leads to faster heat releasing, which may account for the shorter ignition delay observed experimentally.

Based on the above comparisons, the higher reactivity of TMEDA towards NO<sub>2</sub> is due to the formation and oxidation of the C-C double bond on the ethyl linker. The C-H bond adjacent to N atom is easier to break due to the lone pair stabilization, and TMEDA has two such C-H bonds on the ethyl linker, favoring formation of a double bond intermediate that can undergo further oxidization. The double bond can also be opened and oxidized by nitric acid.

In contrast, although TMMDA has five carbon atoms adjacent to N atoms, they are not connected to each other, so that formation of a C-C double bond is impossible for TMMDA. The same mechanism can also be applied to explain the reactivity difference between DMPipZ and TMTZ, where DMPipZ has two adjacent carbons leading to short ignition delay, while TMTZ has no pairs of adjacent carbons and is non-hypergolic.

## **6. Comparison between the initiation of diamines (TMEDA and TMMDA) and their dinitrate salts (TMEDADN and TMMDADN)**

To illustrate how salt formation affects the reactivity of these fuels, we calculated the H-abstraction by NO<sub>2</sub> from the TMEDA (TMMDA)-dinitric acid complex in gas phase, as shown in

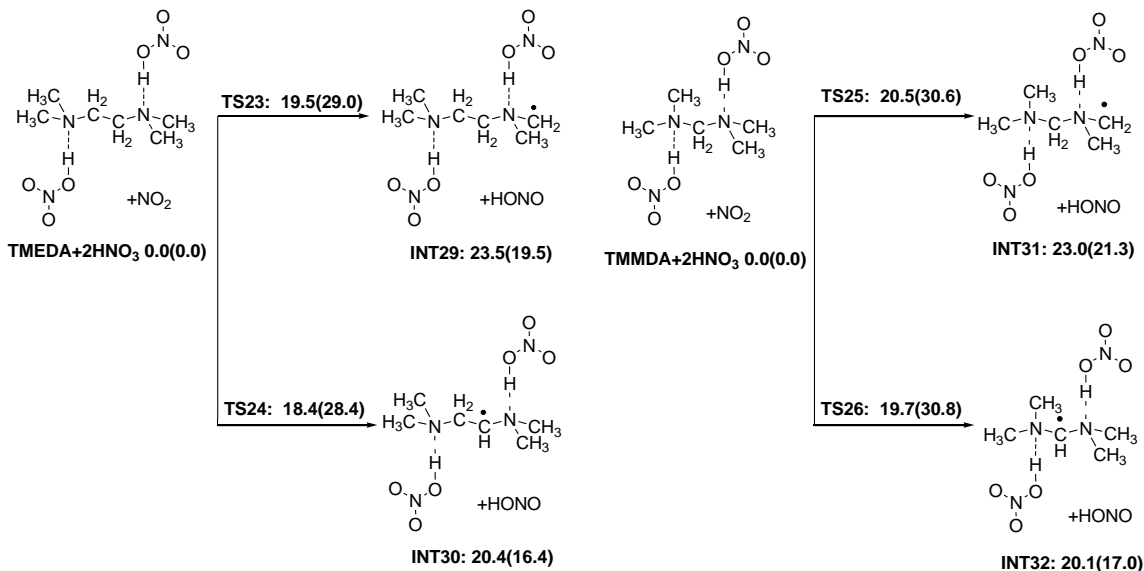


**Figure 4-7.** Initiation reactions between TMEDA(TMMDA)-2HNO<sub>3</sub> complex and NO<sub>2</sub>. The enthalpy and Gibbs free energy (in parentheses) of each species are provided in kcal/mol.

Figure 4-7. Without solvent stabilization, proton transfer and salt formation are not favored in vacuum, as indicated by the longer N-H distance (1.580Å in TMEDA-2HNO<sub>3</sub> and 1.665Å in TMMDA-2HNO<sub>3</sub>) and shorter O-H distance (1.049Å in TMEDA-2HNO<sub>3</sub> and 1.030Å in TMMDA-2HNO<sub>3</sub>). However, although the proton transfer and salt formation are not as complete for gas phase as for the polar solvent, we still observe considerable chemical differences between amine and the amine-HNO<sub>3</sub> complex, which provides insight about the reactivity of TMEDADN and TMMDADN with fully transferred protons.

TS geometries of H-abstraction on two amine-HNO<sub>3</sub> complexes are shown in Figure 4-8. The barriers for these reactions are ~10 kcal/mol higher than those for the pure amines. The final amine-HNO<sub>3</sub> radicals (INT29-32) are also ~8 kcal/mol less stable than the pure amine-radicals (INT1, INT2, INT 20 and INT21), which can be explained as follows. As indicated in Section 2 and 3, lone pairs on N play an important role on lowering the barriers of H-abstraction by donating electron density into the antibonding orbital of adjacent C-H bonds. In amine-HNO<sub>3</sub> complexes, the electron density of lone pair of N is drawn to the proton on the nitric acid and less

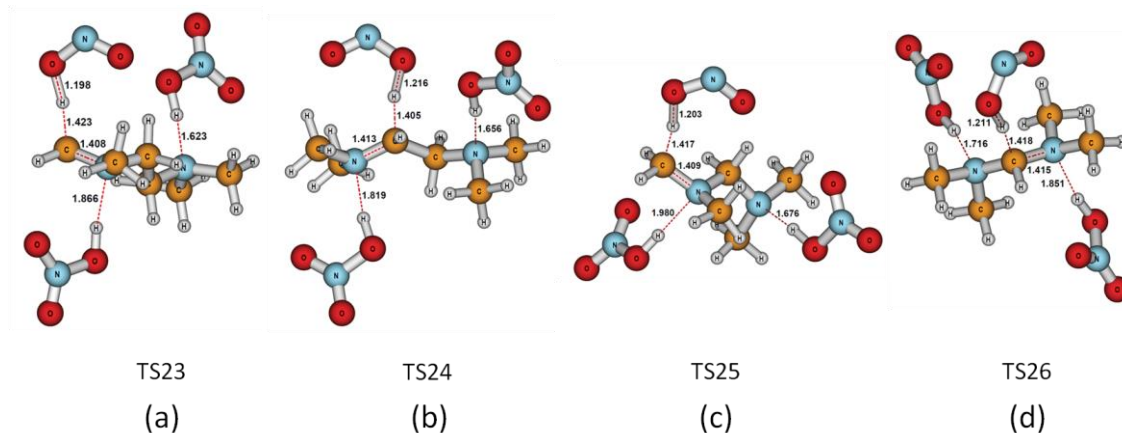


**Figure 4-8.** Structures of (a)TS23 (b)TS24 (c)TS25 (d)TS26

capable of donating into the C-H antibonding orbital, resulting in higher barriers and less stable final products. At TS23-25, the N-H distances on the side at which H-abstraction is taking place are  $\sim 0.2\text{\AA}$  longer than the N-H bond distances on the other side, indicating that the C-H antibonding orbital is competing with the N-H bond for the electron density of lone pair on N, pushing the proton away from N and leading to the extra energy cost for reaction to proceed. It is reasonable to conclude that when protons are fully transferred, the lone pair on N is more confined and localized in the N-H bond region and not able to interact with nearby vacant orbital or free radicals, resulting in even higher barrier and endothermicity of H-abstraction. In other words, the salt formation uses the lone pair electrons on N to form N-H bonds while the product salt is similar to the corresponding alkane, which is chemically inert. This leads to the dinitrate salt playing a less important role in the early stage of ignition.

## Conclusion

DFT calculations of energetics for various reactions involved in the hypergolic reaction of  $\text{HNO}_3$  with TMEDA and TMMDA lead to an atomistic chemical mechanism that explains the dramatic

difference in pre-ignition delay between these two fuels. We find two key factors and illustrate how the molecular structure relates to the ignition delay.

- The first factor is the exothermicity of the formation of the dinitrate salt of TMEDA and TMMDA. Due to the shorter distance between basic amines in TMMDA, it is more difficult to protonate both amines for the stronger electrostatic repulsion, resulting in the heat of dinitrate salt formation being smaller by 6.3 kcal/mol.
- The second factor is the reaction rate of TMEDA and TMMDA reacting with NO<sub>2</sub> to the step that releases sufficient heat and additional reactive species to propagate reaction. In TMEDA, the formation of the intermediate with C-C double bond and the low bond energy of C-C single bond provide a route with low barrier to oxidize C.

Both factors can contribute to the shorter ignition delay of TMEDA. The same reasoning based on the molecular structure can be applied to other fuels, such as DMPipZ and TMTZ. These results indicate that TMEDA and DMPipZ are excellent green replacements for hydrazines as the fuel in bipropellants.

## References

1. Catoire, L.; Chaumeix, N.; Pichon, S.; Paillard, C., *J. Propul. Power* **2006**, 22 (1), 120-126.
2. Osmont, A.; Catoire, L.; Klapotke, T. M.; Vaghjiani, G. L.; Swihart, M. T., *Propellants Explosives Pyrotechnics* **2008**, 33 (3), 209-212.
3. Pichon, S.; Catoire, L.; Chaumeix, N.; Paillard, C., *J. Propul. Power* **2005**, 21 (6), 1057-1061.
4. Nonnenberg, C.; Frank, I.; Klapotke, T. M., *Angew. Chem., Int. Ed.* **2004**, 43 (35), 4585-4589.

5. Frota, O. M., B.; Ford, M., *Proceedings of the 2nd International Conference on Green Propellants for Space Propulsion (ESA SP-557)*. **2004**.
6. Co., P. P., Petroleum Derivable Nitrogen Compounds as Liquid Rocket Fuels. In *Report 1478-56R, Phillips Petroleum Co*, 1956.
7. Wang, S. Q.; Thynell, S. T.; Chowdhury, A., *Energy Fuels* **2010**, *24*, 5320-5330.
8. Wang, S. Q.; Thynell, S. T., *unpublished result. The experimental setting to measure the ignition delay is the same as described in Ref 4* **2010**.
9. McQuaid, M. J.; Stevenson, W. H.; Thompson, D. M., *Proceedings for the Army Science Conference (24th)* **2005**.
10. Chen, C.-C.; Nusca, M. J.; McQuaid, M. J. *Modeling Combustion Chamber Dynamics of Impinging Stream Vortex Engines Fueled with Hydrazine-Alternative Hypergols*; 2008.
11. Addison, C. C., *Chem. Rev. (Washington, DC, U. S.)* **1980**, *80* (1), 21-39.
12. Stone, D. A., *Toxicol. Lett.* **1989**, *49* (2-3), 349-360.
13. Klapotke, T. M.; Harcourt, R. D.; Li, J. B., *Inorg. Chim. Acta* **2005**, *358* (14), 4131-4136.
14. McQuaid, M. J.; Ishikawa, Y., *J. Phys. Chem. A* **2006**, *110* (18), 6129-6138.
15. Catoire, L.; Chaumeix, N.; Paillard, C., *J. Propul. Power* **2004**, *20* (1), 87-92.
16. Bedford, G.; Thomas, J. H., *Journal of the Chemical Society-Faraday Transactions I* **1972**, *68* (11), 2163-2170.

## Chapter 5

### THEORETICAL INVESTIGATIONS OF EARLY REACTIONS OF MONOMETHYLHYDRAZINE WITH MIXTURES OF NO<sub>2</sub> AND N<sub>2</sub>O<sub>4</sub>

#### Overview

Hypergolic bipropellants are fuel-oxidizer combinations that ignite spontaneously upon mixing at ambient temperatures. They facilitate the design of rocket thrusters by simplifying the ignition system, and are widely used in propulsion systems in which variable and/or intermittent thrust capabilities are needed. Among the most commonly deployed bipropellant combinations is monomethylhydrazine/nitrogen tetroxide, which is also referred to as MMH/NTO or CH<sub>3</sub>NHNH<sub>2</sub>/N<sub>2</sub>O<sub>4</sub>.<sup>1</sup> For applications in which the freezing point of NTO is too high, an alternative oxidizer is red fuming nitric acid (RFNA), which is composed of nitric acid (HNO<sub>3</sub>, ~85 wt%) and NO<sub>2</sub> (8-15 wt%).

Recently the impinging stream vortex engine (ISVE) has attracted significant attention due to its compact size and potential for efficient combustion, making it important to develop computational fluid dynamics (CFD) models to gain insight into the influence of design parameters on engine performance.<sup>2-5</sup> An important part of this effort is to develop a chemical kinetics mechanism for MMH/NTO or MMH/RFNA combinations.

To provide a starting point for such activities a detailed, finite-rate, chemical kinetics mechanism of MMH/RFNA was developed by the U.S. Army Research Laboratory (ARL)<sup>6-9</sup> for modeling the gas-phase combustion processes. The most recent version of this mechanism involves 513 reactions and 81 species.<sup>6</sup> Sources for the ARL mechanism include the following:

1. A set of reactions for H/C/N/O compounds developed by Anderson and co-workers for modeling the dark zones observed in solid-propellant combustion (43 species, 204 reactions),<sup>10</sup>
2. Approximately 160 small-hydrocarbon-molecule reactions that were extracted from the GRI 3.0 database,<sup>11</sup>
3. Approximately 80 reactions involving HNO<sub>3</sub>, NO<sub>3</sub>, N<sub>2</sub>O<sub>4</sub>, and hydrocarbon/NO<sub>x</sub> moieties that were identified via a literature search performed specifically for the mechanism development effort, and
4. Approximately 50 reactions recommended by Catoire and co-workers for modeling the ignition and combustion of MMH/O<sub>2</sub><sup>12</sup> and MMH/NTO<sup>13</sup> systems.

The validity and completeness of the ARL mechanism was tested by running CHEMKIN<sup>14</sup> simulations for MMH/NTO systems, and a reduced version of the mechanism was used in CFD simulations for the ISVE engine.<sup>2, 5, 8</sup>

One major concern with the ARL MMH/RFNA mechanism is the lack of relevant experimental studies for its validation.<sup>6</sup> As part of an effort to provide experimental support for this mechanism, we investigated the pre-ignition reactions between MMH and HNO<sub>3</sub> (the major constituent of RFNA) in an earlier work.<sup>15</sup> These experimental results suggested that the current MMH/RFNA mechanism omits some important early reactions between MMH and HNO<sub>3</sub> and corresponding species. Since NO<sub>2</sub>/N<sub>2</sub>O<sub>4</sub> is another important constituent in RFNA, its early gas-phase reactions with MMH are examined in this work.

The current ARL mechanism for MMH/NTO, a subset of the MMH/RFNA mechanism, contains reactions categorized in two domains: 1. single-bond fission events to strip fragments from MMH and generate free radicals, and 2. radical-radical reactions to form either closed-shell or open-shell species.

Given the low temperature (<100°C) in the pre-ignition environment, direct bond fission from MMH to produce H, CH<sub>3</sub> or NH<sub>2</sub> is unlikely so that NO<sub>2</sub> is the major free radical available initially. Based on this assumption, the ARL mechanism considers the two types of initial reactions: 1. H-abstraction from MMH and sequential HONO formations, and 2. recombination between NO<sub>2</sub> and MMH free radicals generated by H-abstraction.

However, these reactions do not fully explain the formation of a condensate that has been observed in several previous studies involving examinations of a residue from gas-phase reactions in a stoichiometric mixture of MMH and NO<sub>2</sub>/N<sub>2</sub>O<sub>4</sub>.<sup>16</sup> The IR properties of this residue are quite similar to the IR properties of a residue obtained from reactions between liquid-phase MMH and gaseous NO<sub>2</sub>/N<sub>2</sub>O<sub>4</sub>.<sup>17</sup> The IR properties of the residue from these two studies suggest that monomethylhydrazinium nitrate (MMH•HNO<sub>3</sub>) is formed in addition to other species.<sup>16</sup> The formation of MMH•HNO<sub>3</sub> was also detected by Saad et al.,<sup>18</sup> who examined liquid-phase reactions between MMH and N<sub>2</sub>O<sub>4</sub> in a system diluted by CCl<sub>4</sub> at -20°C. In a recent work by Catoire et al.,<sup>13</sup> it is suggested that the MMH•HNO<sub>3</sub> detected as a major product in the residue by Semans et al. is not formed from reactions in the gas phase, since its elemental analysis matches rather poorly with that of the residue as determined by Breisacher et al.<sup>19</sup> Catoire et al. suggests that nonionic compounds are formed and accumulate in a condensate. However, it appears that no experiments were carried out to confirm the formation of these nonionic compounds.

Based on the above discussion, there is a clear need to reexamine gas-phase reactions between MMH and NO<sub>2</sub>/N<sub>2</sub>O<sub>4</sub> at low temperatures in order to identify the relevant preignition products and reaction pathways. There are two objectives with the present work. First, we would like to experimentally identify *in situ* the species formed early in the preignition event from gas-phase reactions between MMH and NO<sub>2</sub>/N<sub>2</sub>O<sub>4</sub>. Second, we would like to use quantum mechanics (QM)

tools to help elucidate the reaction pathways, since experimentally it is rather difficult to identify and quantify radicals, as well as to identify transition-state structures.

### Computational details

The geometry optimization and Hessian calculation were carried out at the level of M06-2X/6-311++G\*\*. <sup>20</sup> The Hessian was used to provide the vibrational frequencies for zero-point energy (ZPE) and thermocorrections to enthalpy and entropy. In addition, at these optimized geometries we calculated the energy at the UCCSD(T)/6-31G\*\* level of QM. In the reaction of HONO formation, the ONO-H distance is the key reaction coordinate and sensitive to different functionals. Comparing with geometries at transition state (TS) from CCSD/6-31+G\*\* reported by McQuaid and Ishikawa,<sup>7</sup> the greatest difference in O-H distance is at the TS of reaction to form CH<sub>3</sub>NNH<sub>2</sub>+HONO (2.170 v.s 1.908Å), and for the remaining, the difference in O-H is less than 0.1Å. These geometries differences, however, do not cause much difference in barrier heights of HONO formation, as shown in section 4.1. All TS were shown to have exactly one negative eigenvalue by following the minimum energy path (MEP) scan to connect reactant and product. Free energies are reported at 298.15 K and 1 atm.

For reactions inside the aerosol or on the aerosol surface, we added the electrostatic interaction between reactants and surrounding ions with Poisson-Boltzmann solvation model (implicit solvent) implemented in Jaguar,<sup>21</sup> using a dielectric constant of 80.37 and a spherical cavity of radius 1.40Å for water. We consider that the solvation effects calculated for water represent the high dielectric properties expected for these systems, with the results depending little on the exact values as long as the dielectric constant is greater than 20 and radius smaller than 2.8Å. All geometry optimizations, solvation and Hessian calculations were carried out with Jaguar 7.6.<sup>22</sup> The UCCSD(T) calculation was done with NWChem.<sup>23, 24</sup>

## 1. H-atom abstraction from MMH

The oxidation of MMH via sequential HONO formation and the final  $N_2$  generation were studied computationally as shown in Figure 5.1. The first H-abstraction from MMH has been studied in detail by McQuaid and Ishikawa,<sup>7</sup> who reported barrier heights for H-abstractions from three different positions (H on N-CH<sub>3</sub> and two H on N-NCH<sub>3</sub> - *cis* and *trans* to the methyl group, respectively) to form *cis*-HONO are 10.1, 10.6 and 11.2 kcal/mol (without ZPE or thermocorrections) at CCSD(T)/6-311+G(2df,p)//CCSD/6-31+G(d,p) level relative to free NO<sub>2</sub> and MMH.

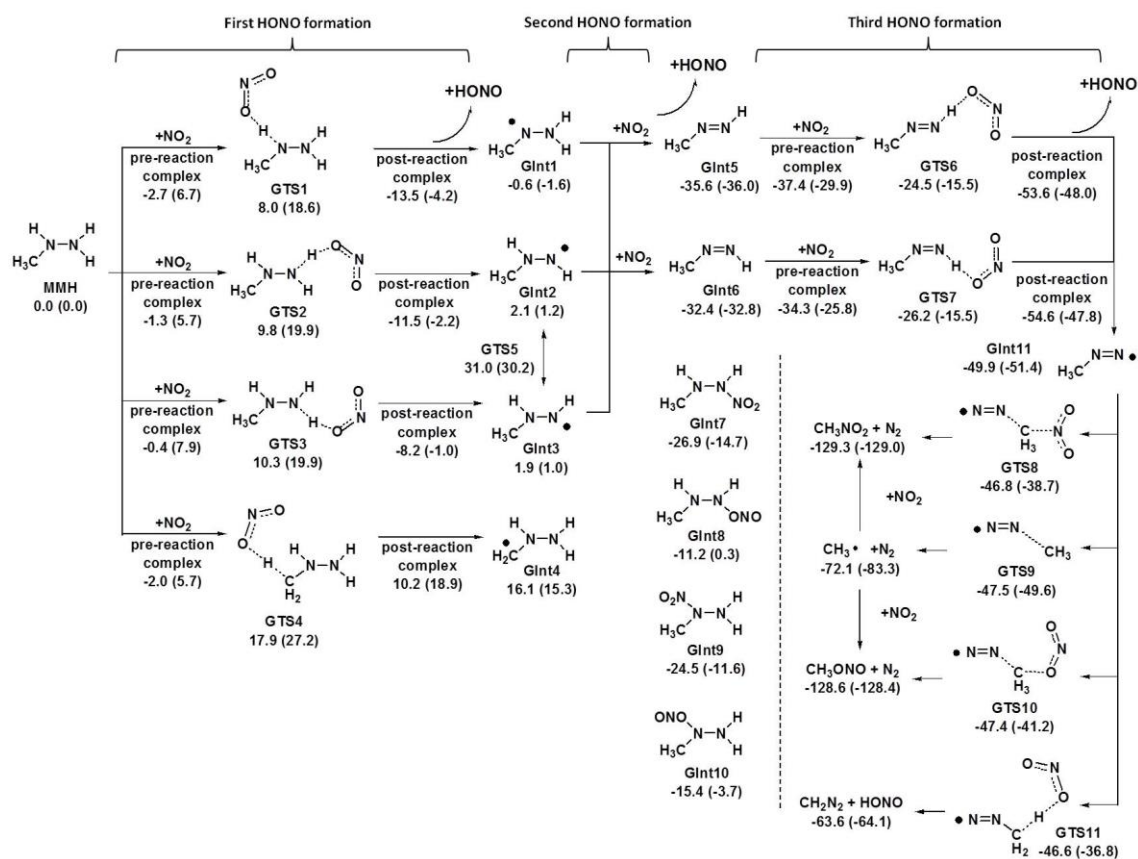


**Figure 5-1.** Reactions between MMH and NO<sub>2</sub> in gas phase. Barriers of all H-abstractions from N of MMH to form HONO are about 10 kcal/mol, and the same H-abstraction from methyl group is 16.1 kcal/mol endothermic and has ~10 kcal/mol higher barrier, rendering the oxidation of carbon slower at low temperature. Enthalpies and Gibbs free energies (in the parentheses) are calculated at 298.15K and 1 atm. *cis*-HONO at standard state is used as reference product.

These results are close to our values of 8.0, 9.8 and 10.3 kcal/mol (including ZPE and temperature corrections, relative to free NO<sub>2</sub> and MMH). We find that the most readily abstracted H-atom is from the nitrogen with the methyl group, in agreement with the previous study. The binding energy between the product HONO and the free radical is substantial (10-13 kcal/mol enthalpy), reducing the free energy of the post-reaction complex to even lower levels than the unbound free radicals GInt1 – GInt3. However, in normal experimental conditions the partial pressure of HONO is usually much lower than 1 atm (the reference state), favoring the formation of unbound free radicals, after taking concentration correction into account. The interconversion between GInt2 and GInt3 via N-N bond rotation has a high barrier (~29 kcal/mol) because the N-N bond has some double-bond character due to the delocalization of the N lone pair. Abstraction of an H atom from a methyl group (GTS4) is ~10 kcal/mol higher in energy than from N atoms. Furthermore, this reaction is 16.1 kcal/mol endothermic, in contrast to H-abstractions from N atoms, which are almost thermoneutral. Therefore H-atom abstraction from the methyl group will not play an important role during the pre-ignition event, and experimentally we observed abundant methyl-containing compounds, indicating the inertness of methyl group at room temperature. Consequently reactions beyond GInt4 are not considered in Scheme 1.

## **2. H-atom abstraction from CH<sub>3</sub>NNH<sub>2</sub> or CH<sub>3</sub>NHNH**

The H-abstraction reactions from either CH<sub>3</sub>NNH<sub>2</sub> or CH<sub>3</sub>NHNH very likely have no barrier because of stabilization of the N *p* orbital bonded to the H with delocalization of the adjacent N lone pair. Indeed we could not find a transition state in the electronic energy surface despite an exhaustive search. The free energy surface after including ZPE might well lead to a barrier. Ishikawa and McQuaid,<sup>9</sup> using the MPWB1K functional, found that 1-2 kcal/mol of kinetic energy is enough to activate H-atom abstraction, indicating very low barriers for H-abstraction. GInt7 - GInt10 are products from recombination between two radicals (GInt1 - GInt3 and NO<sub>2</sub>). All of

them are enthalpically and entropically less stable than the product of HONO formation, GInt5 and GInt6. Experimentally these recombination products are not detected, suggesting that for these two bimolecular processes, the reaction cross-section of HONO formation is much greater than that of recombination.

### 3. H-atom abstraction from $\text{CH}_3\text{N}=\text{NH}$

The enthalpic barrier for the H-atom abstraction is 11.1 kcal/mol for *anti*- $\text{CH}_3\text{N}=\text{NH}$  (GInt5 $\rightarrow$ GTS6 $\rightarrow$ GInt11) and 6.2 kcal/mol for *syn*- $\text{CH}_3\text{N}=\text{NH}$  (GInt6 $\rightarrow$ GTS7 $\rightarrow$ GInt11). The  $\text{CH}_3\text{N}=\text{N}$  radical (GInt11) can either break the C-N bond to release  $\text{N}_2$  and  $\text{CH}_3$  radical (ARL mechanism reaction No. 456) with only 2.4 kcal/mol barrier, or undergo  $\text{NO}_2$  attack at different orientations to form  $\text{CH}_3\text{ONO}$  and  $\text{CH}_3\text{NO}_2$  with barrier heights 2.5 and 3.1 kcal/mol, respectively.

Since the measured concentration of  $\text{CH}_3\text{ONO}_2$  is much larger than both  $\text{CH}_3\text{NO}_2$  and  $\text{CH}_3\text{ONO}$ , and the  $\text{NO}_2$  concentration is much larger than the concentration of  $\text{ONONO}_2$ , the major fraction of the formation of  $\text{CH}_3\text{ONO}_2$  is not from reactions involving either  $\text{CH}_3$  or  $\text{CH}_3\text{NN}$ . For example, reactions between  $\text{CH}_3$  and  $\text{NO}_2$  forming the methoxy group and  $\text{NO}$  are not likely since the concentration of  $\text{NO}$  is quite small. In addition, the formation of  $\text{CH}_2\text{N}_2$  via H-abstraction from methyl group is also found to have a low barrier (3.3 kcal/mol). However, this product was not detected experimentally, indicating that the direct dissociation of methyl free radical from GInt11 may be much faster than other bimolecular pathways.

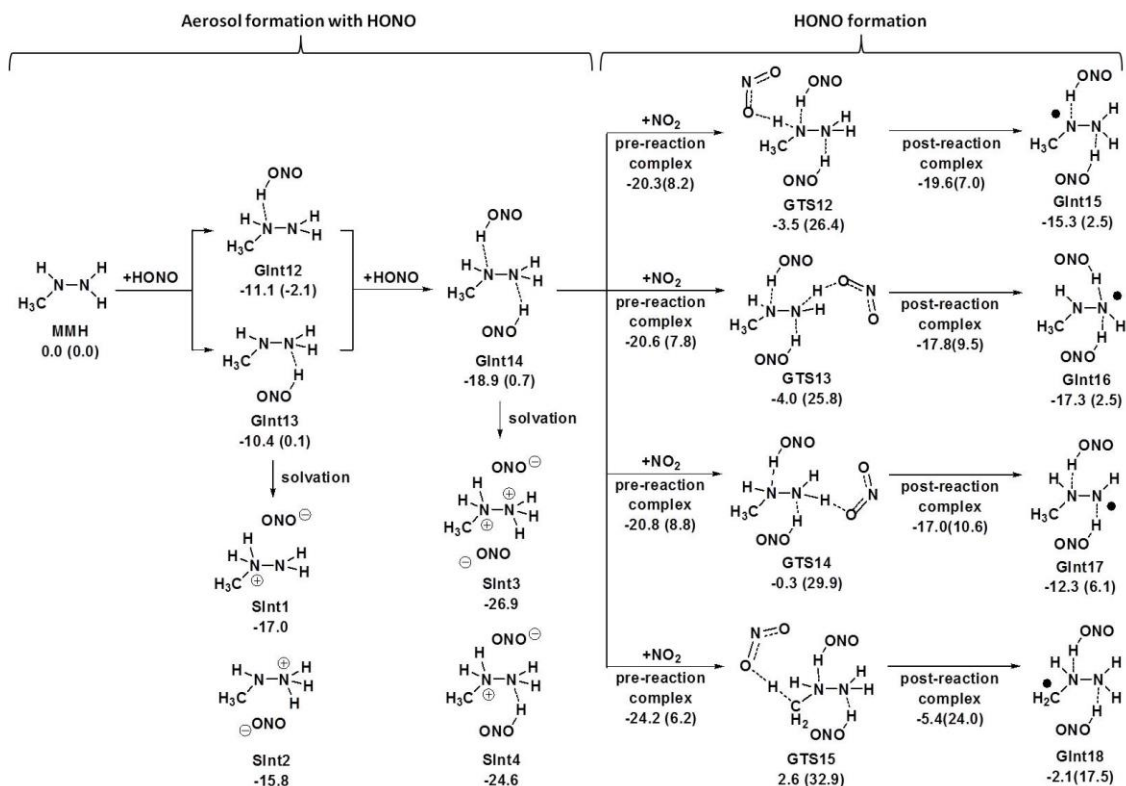


**Figure 5-2.** The formation of aerosol MMH•HONO and MMH•2HONO followed by H-abstraction and HONO formation. The barriers of H-abstraction from MMH•2HONO aerosol are 7~9 kcal/mol higher than the ones from MMH. Enthalpies and Gibbs free energies (in the parentheses) are calculated at 298.15K and 1 atm. *cis*-HONO at standard state is used as reference product.

#### 4. Formation of MMH•HONO aerosol and its lower reactivity

In each step of Figure 5-1, HONO is produced, which is able to form aerosol with unreacted MMH because the basic N atoms on MMH are able to accept a proton from HONO. As shown in Figure 5-2, protons in MMH•HONO complexes in gas phase prefer to stay on HONO. The enthalpies to form  $n$ HONO•MMH complexes ( $n=1,2$ ) are roughly additive (-21.5 kcal/mol from the sum of enthalpy of GInt12 and 13 vs. -18.9 kcal/mol of GInt14) and the free energies to form these complexes are about thermoneutral (-2.1, 0.1 and 0.7 kcal/mol for GInt12, GInt13 and GInt14). In the strong solvation environment (in the aerosol), the proton transfer from HONO to MMH is more

avored and exothermic, which accounts for the observation of  $\text{ONO}^-$  anion in the IR spectra. However, the reaction heat to transfer one and two protons from the  $\text{MMH}\cdot\text{2HONO}$  complex in a solvated system differ little (5.7 vs. 8.0 kcal/mol exothermic), unlike complexes in the gas phase. It is because in  $\text{SInt3}$  with two protons fully transferred to N atoms the electrostatic repulsion between two positively charged N centers partially cancels the energy gain from the neutralization. Hence, the pathways for continued growth and composition of the aerosol can be either  $\text{MMH}^{2+}\cdot\text{2ONO}^-$  or  $\text{MMH}^+\cdot\text{ONO}^-$ . In the oxidizer-rich case, however, the former composition is more likely. The spontaneous nucleation in gas phase followed by the exothermic growth make the aerosol formation a rapid process as observed in the experiment.

We also found that the  $\text{MMH}\cdot\text{HONO}$  aerosol is less reactive than free MMH. Reactions to abstract H from  $\text{MMH}\cdot\text{HONO}$  complex have barriers 7~9 kcal/mol higher than the same H-abstraction from MMH. The reason is that in free MMH, the lone pairs on the N can stabilize the transition state via resonance, whereas such stabilization is less available when lone pairs donate electron density to the proton, resulting in a higher barrier. The increase of the barrier for HONO formation resulting from the salt formation was also observed in the case of alkylamine and nitric acid.<sup>25</sup> As a result, growth of the particles is favored over H-abstraction reactions at the low temperatures of our experiments. As the temperature increases, particles will either undergo H-abstraction reactions or evaporate into MMH and HONO so that particles will shrink and eventually disappear. Such a phenomenon of particle disappearance is observed just prior to ignition in the  $\text{MMH}\cdot\text{HNO}_3$  reaction system.<sup>15</sup>

## 5. Reactions of asymmetric dimer of $\text{NO}_2$ , $\text{ONONO}_2$ in gas phase

The formation of  $\text{ONO}_2^-$  and  $\text{CH}_3\text{ONO}_2$  cannot be explained by simple H-atom abstractions or recombination of the radical intermediates with  $\text{NO}_2$ . One potential source of nitrate is from the

isomerization of  $N_2O_4$ . It is known that liquid  $NO_2$  dimerizes to form  $N_2O_4$  and disproportionates into  $NO^+$  and  $NO_3^-$ .<sup>26</sup>  $NO_2$  can also react with water vapor to give HONO and  $HNO_3$ . Finlayson-Pitts and coworkers<sup>27</sup> proposed that the asymmetric isomer ONONO<sub>2</sub> is the key intermediate as the source of nitrate. Our previous study shows that the reaction to form ONONO<sub>2</sub> has low enthalpic barrier (<5 kcal/mol),<sup>28</sup> which means equilibrium between  $NO_2$  and ONONO<sub>2</sub> is very fast. Recently Lai et al.<sup>29</sup> also found that ONONO<sub>2</sub> can play an important role in the hypergolic reaction between hydrazine and liquid NTO. We would also like to check if ONONO<sub>2</sub> plays a similar role in the gas phase reaction between MMH and  $NO_2$ .

The easiest reactions between MMH and trans-ONONO<sub>2</sub> is the new N-N bond formation between  $NO^+$  and electron-rich N atoms on MMH followed by the proton transfer from N-H bond to  $NO_3^-$  to form nitric acid, as shown in Figure 5-3. Although it is very easy to form nitric acid (enthalpic barrier is about 1 kcal/mol), to form methyl nitrate is difficult in gas phase (34 kcal/mol enthalpic barrier) due to the unfavorable charge separation (nitrate anion has to attack from the back of methyl group, which is far from the positive N center). Therefore, the gas phase reactions between MMH and ONONO<sub>2</sub> can easily generate  $HNO_3$  and explain the experimental observation of  $NO_3^-$ , however, they cannot explain the abundant  $CH_3ONO_2$  observed in the IR spectrum, which we

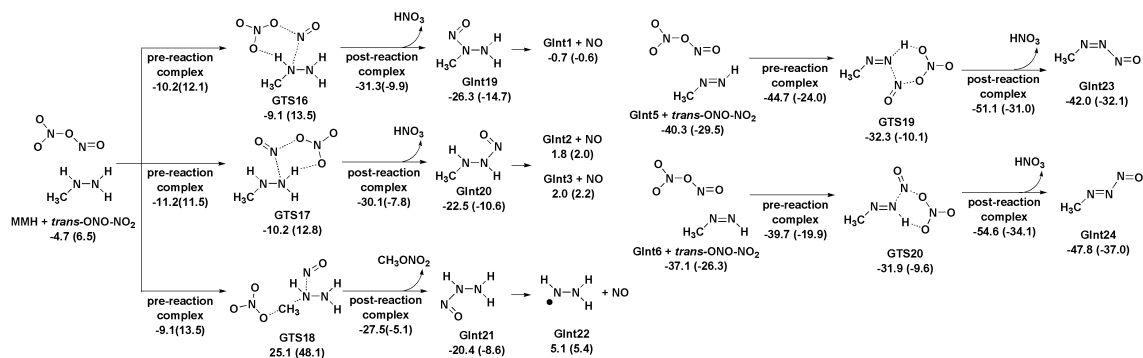


**Figure 5-3.** The reactions between ONONO<sub>2</sub>, MMH, Gint5 and Gint6 in gas phase. These reactions have low barriers and produce HNO<sub>3</sub> as the source of nitrate anion observed experimentally. Enthalpies and Gibbs free energies (in the parentheses) are calculated at 298.15K and 1 atm. *cis*-HONO at standard state is used as reference product.

surmised to be produced on the surface of aerosol, as studied in the section 4.6. ONONO<sub>2</sub> can also react with intermediates from HONO formation, such as GInt5 and GInt6, as shown in Figure 5-3. N atoms on GInt5 and GInt6 are *sp*<sup>2</sup> hybridized, not as electron-rich as the *sp*<sup>3</sup> hybridized ones, therefore barriers to abstract H from GInt5 and GInt6 to form HNO<sub>3</sub> are about 10 kcal/mol higher than H-abstractions from MMH.

## 6. Reactions facilitated by aerosol to form CH<sub>3</sub>ONO<sub>2</sub>

Several experiments indicate that NO<sub>2</sub> can react with water or alcohol heterogeneously (surface-catalyzed)<sup>27, 30-32</sup>, probably via the same ONONO<sub>2</sub> intermediate<sup>27</sup>. The aerosol of ONO<sup>-</sup> and MMH

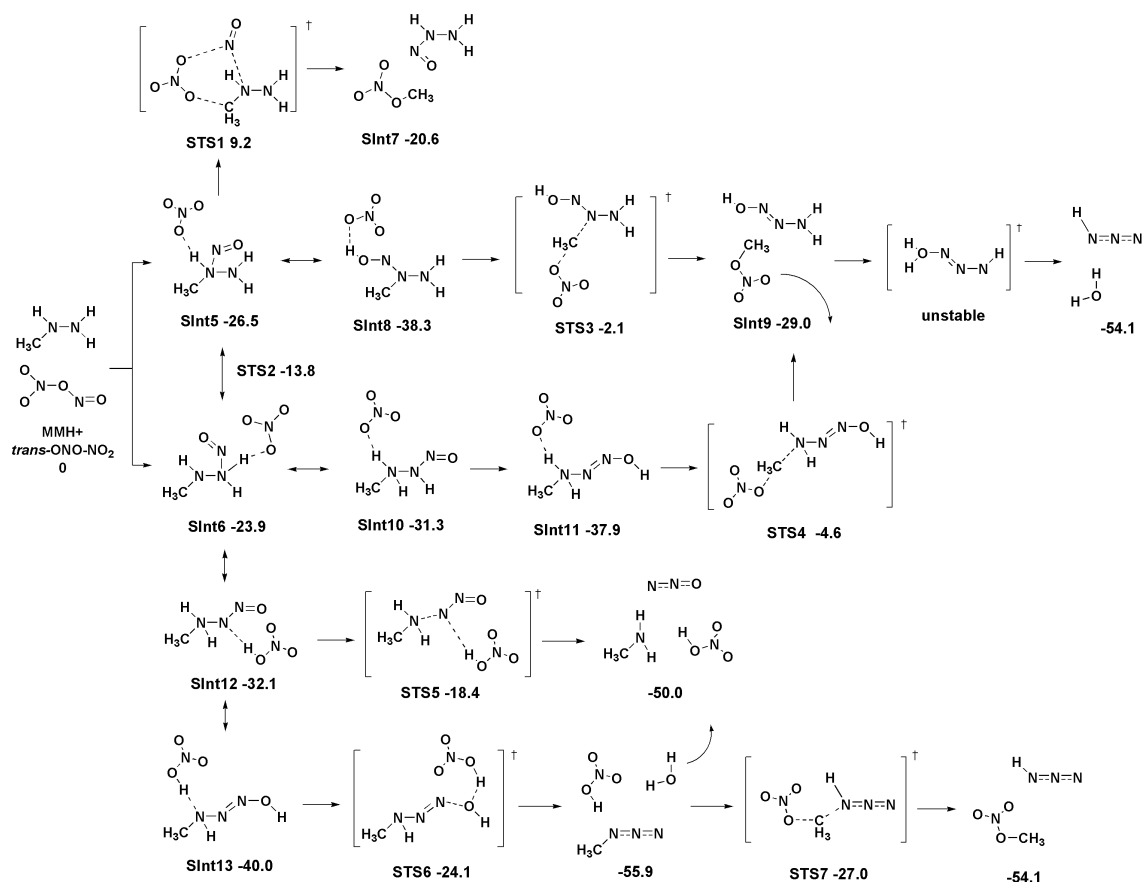


**Figure 5-4.** The reactions between ONONO<sub>2</sub> and MMH in water to simulate potential energy surface in the aerosol. Enthalpies is calculated at 298.15K and 1 atm. Several gas products, such as CH<sub>3</sub>ONO<sub>2</sub> and N<sub>2</sub>O, can desorb from the aerosol and be observed via IR spectra.

cation (such as Sint1-Sint4) provides polar ionic surface that can stabilize the asymmetric ONONO<sub>2</sub> and promote nitrate formation. This pathway can be favored at higher NO<sub>2</sub> concentrations because ONONO<sub>2</sub> concentration is proportional to [NO<sub>2</sub>]<sup>2</sup>, which also explain the experimental observation that the formation of methyl nitrate was only observed in the NO<sub>2</sub>-rich atmosphere. Since asymmetric ONONO<sub>2</sub> has high dipole moments (3.45D for *cis* and 2.96D for *trans* at B3LYP/6311G\*+ level),<sup>28</sup> we expect the concentration of ONONO<sub>2</sub> to be greatly increased if it is absorbed on a polar surface or formed a molecular complex with a polar molecule.

To study reactions between ONONO<sub>2</sub> and MMH on the polar surface or the sub-surface of the aerosol, we used an implicit solvation model to include the interaction between reactants and surrounding ions. Our proposed reaction mechanism between MMH and ONONO<sub>2</sub> and the corresponding enthalpies are shown in Figure 5-4.

In solution phase, ONONO<sub>2</sub> has strong tendency to dissociate into NO<sub>3</sub><sup>-</sup> and NO<sup>+</sup> with the presence of electron-rich MMH. The electron-deficient NO<sup>+</sup> makes N-N bond with the electron-rich N, preferably the methyl substituted N, on MMH to form SInt5 and SInt6. From SInt5, nitrate anion can attack from the back methyl group to form methyl nitrate with 35.7 kcal/mol barrier.

Once the N-N bond is formed, the acidity of the adjacent N-H bond increases and the overall complex is similar to the salt generated from the neutralization between HNO<sub>3</sub> and corresponding amine. We assumed that the proton transfer in such a polar environment has a low barrier. Therefore, to study tautomers as intermediates is enough to depict the potential energy surface. In our calculations, these tautomers are tightly constrained to conserve the number of protons, while in aerosol, protons can exchange with the environment, implying our barriers should be the upper bounds of true barriers.

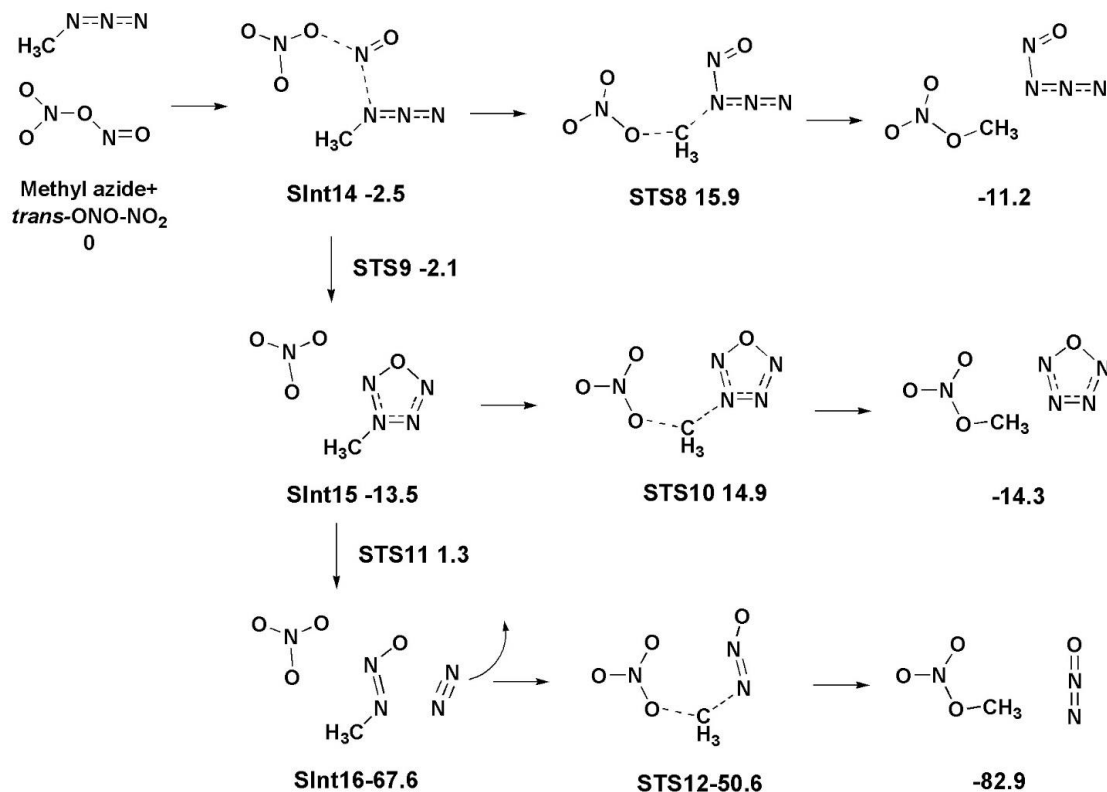


**Figure 5-5.** The reactions between  $\text{CH}_3\text{N}_3$  and  $\text{ONONO}_2$  in water to simulate potential energy surface in the aerosol. The reaction path via SInt14, SInt15, SInt16 and STS12 has low barriers to form  $\text{CH}_3\text{ONO}_2$ . Enthalpies is calculated at 298.15K and 1 atm.

Even with free nitrate anion in aerosol, the barriers for the nucleophilic substitution of the methyl group on MMH are considerable. Among several possible tautomers, SInt8 and SInt11 are the easiest two to form  $\text{CH}_3\text{ONO}_2$  via STS3 and STS4 to SInt9, with barriers 36.2 and 33.3 kcal/mol, respectively, giving the final products, hydrazoic acid and water. See SI for other tautomers and corresponding TS to form  $\text{CH}_3\text{ONO}_2$ . It is also possible to form  $\text{N}_2\text{O}$  and methyl amine by breaking the N-N bond in SInt12 via STS5 with 13.7 kcal/mol barrier, corresponding to the experimental observation of  $\text{N}_2\text{O}$ .

An easier path to form  $\text{CH}_3\text{ONO}_2$  involves the intermediate  $\text{CH}_3\text{N}_3$  formed from SInt13 via STS6 with 15.9 kcal/mol enthalpic barrier. As shown in Figure 5-5, in solution phase,  $\text{CH}_3\text{N}_3$  reacts with  $\text{ONONO}_2$  to form a 5-member ring intermediate (SInt15) with negligible barrier, which then

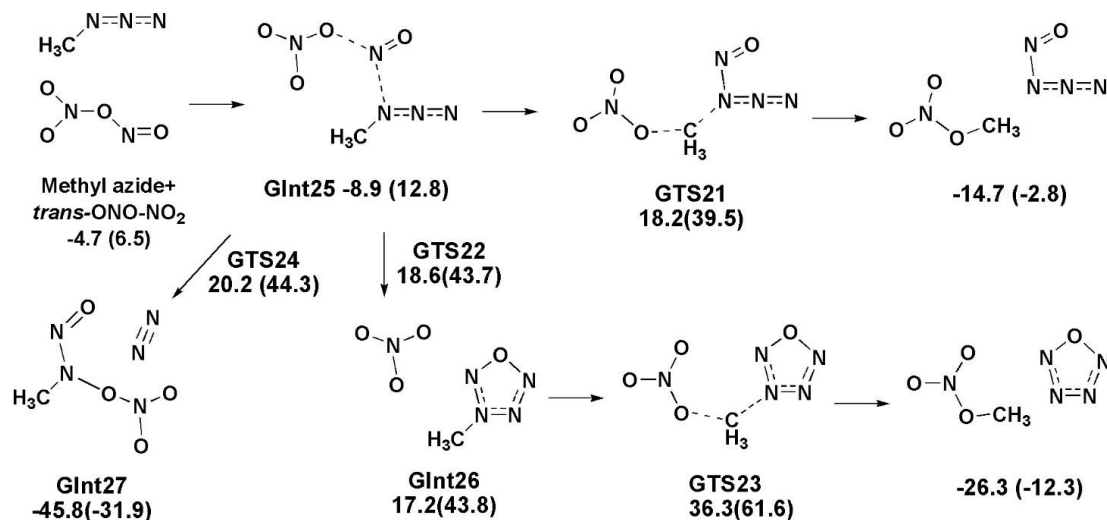


**Figure 5-6.** The reactions between CH<sub>3</sub>N<sub>3</sub> and ONONO<sub>2</sub> in gas phase. All barriers are significantly higher than the corresponding reactions in water, indicating the importance of solvation effect. Enthalpies and Gibbs free energies (in the parentheses) are calculated at 298.15K and 1 atm.

decomposes to release N<sub>2</sub> with 14.8 kcal/mol barrier, and the product (SInt16) undergoes nucleophilic attack of nitrate to form CH<sub>3</sub>ONO<sub>2</sub> and N<sub>2</sub>O with 17.0 kcal/mol enthalpic barrier and 32.3 kcal/mol exothermicity.

The solvation effect plays an important role in facilitating the decomposition of CH<sub>3</sub>N<sub>3</sub> because similar mechanism to produce CH<sub>3</sub>ONO<sub>2</sub> with enthalpic barrier no lower than 24.9 kcal/mol. The barrier to form the same 5-member ring intermediate in gas phase has a 27.5 enthalpic barrier, as shown in Figure 5-6. The STS11-like transition state in gas phase, GTS24, does not connect to a 5-member ring intermediate in the MEP scan, instead it leads to the path to dissociate N<sub>2</sub> from CH<sub>3</sub>N<sub>3</sub> directly, with barrier height 24.9 kcal/mol. These reaction paths do not lead to rapid production of CH<sub>3</sub>ONO<sub>2</sub>. Once N<sub>2</sub>O, CH<sub>3</sub>ONO<sub>2</sub>, and CH<sub>3</sub>N<sub>3</sub> are formed during tautomerization, they can desorb from the aerosol surface and drive reactions further towards completion. The energetics is favorable due to the partial oxidation of MMH. Also the exchange between gas phase and aerosol species is plausible - NO<sub>2</sub> can be absorbed onto the aerosol surface and oxidize

intermediates shown in Scheme 2, leading to a complicated multiphase picture of pre-ignition reactions.

## Conclusions

We studied reactions between MMH and NO<sub>2</sub> vapor in a gold-coated chamber reactor with Fourier transform infrared spectrometry at both MMH-rich and NO<sub>2</sub>-rich conditions. At low concentration of NO<sub>2</sub>, the major products are MMH•HONO and CH<sub>3</sub>N=NH and the minor products are N<sub>2</sub>O, CH<sub>3</sub>N<sub>3</sub>, CH<sub>3</sub>NO<sub>2</sub> and CH<sub>3</sub>ONO. Our QM calculations elucidate possible mechanisms of H-abstraction by NO<sub>2</sub> from MMH to form HONO, which then forms condensate by reacting with MMH in fuel-rich condition. We find that CH<sub>3</sub>N=NH is formed after a second H-abstraction from MMH. Further H-abstraction produces CH<sub>3</sub>ONO, CH<sub>3</sub>NO<sub>2</sub> and N<sub>2</sub>. At higher concentrations of NO<sub>2</sub> the major products are monomethylhydrazinium nitrite and methyl nitrate. The formation of methyl nitrate is attributed to the asymmetric isomer ONONO<sub>2</sub> of N<sub>2</sub>O<sub>4</sub>, which is favored at high NO<sub>2</sub> concentration. Our *ab-initio* calculations indicate that further reactions between MMH and ONONO<sub>2</sub> facilitated by the surface of the aerosol or inside, can generate CH<sub>3</sub>ONO<sub>2</sub>, CH<sub>3</sub>N<sub>3</sub> and N<sub>2</sub>O, products observed in NO<sub>2</sub>-rich experimental conditions. This study illustrates the heterogeneous nature of the pre-ignition reactions between MMH and NO<sub>2</sub>.

## References:

1. Schmidt, E. W., In *Hydrazine and Its Derivatives: Preparation, Properties, Applications* (2<sup>nd</sup> Ed., Vol. 1), Wiley-Interscience: New York, 2001.
2. Nusca, M. J.; Michaels, R. S. In *Utility of Computational Modeling for the study of Combustion Instability in Small MMH-NTO Liquid Rocket Engines*, 43<sup>rd</sup> AIAA/ASME/SAE/ASEE Joint Propulsion Conference and Exhibit, Cincinnati, OH, Cincinnati, OH, 2007.

3. Nusca, M. J.; Michaels, R. S., *Proceedings of the 50<sup>th</sup> JANNAF Propulsion Meeting* **2002**, Vol.1, 179-191.
4. Nusca, M. J. In *Computational Model of Impinging-Stream/Swirl Injectors in a Hypergolic Fuel Engine*, AIAA/ASME/SAE/ASEE Joint Propulsion Conference and Exhibit, Huntsville, AL, Huntsville, AL, 2003.
5. Nusca, M. J.; Michaels, R. S. 40th AIAA/ASME/SAE/ASEE Joint Propulsion Conference, Reston, VA, Institute of Aeronautics and Astronautics (AIAA): Reston, VA, 2004.
6. Anderson, W. A.; McQuaid, M. J.; Nusca, M. J.; Kotlar, A. J. *A Detailed, Finite-Rate, Chemical Kinetics Mechanism for Monomethylhydrazine-Red Fuming Nitric Acid Systems*; ARL-TR-5088; U.S. Army Research Laboratory: Aberdeen, MD, 2010.
7. McQuaid, M. J.; Ishikawa, Y., *J. Phys. Chem. A* **2006**, *110* (18), 6129-6138.
8. Chen, C.-C.; Nusca, M. J.; McQuaid, M. J. *Modeling Combustion Chamber Dynamics of Impinging Stream Vortex Engines Fueled With Hydrazine-Alternative Hypergols*; NTIS-ADA503941; U.S. Army Research Laboratory: Aberdeen Proving Ground, 2008.
9. Ishikawa, Y.; McQuaid, M. J., *Journal of Molecular Structure-Theochem* **2007**, *818* (1-3), 119-124.
10. Vanderhoff, J. A.; Anderson, W. R.; Kotlar, A. J. In *Dark Zone Modeling of Solid Propellant Flames*, Proceedings of 29<sup>th</sup> JANNAF Combustion Subcommittee Meeting, Hampton, VA, Hampton, VA, 1992; pp 225-237.
11. Smith, G. P.; Golden, D. M.; Frenklach, M.; Moriarty, N. W.; Eiteneer, B.; Goldenberg, M.; Bowman, C. T.; Hanson, R. K.; Song, S.; William C. Gardiner, J.; Lissianski, V. V.; Qin, Z. GER-MECH 3.0. [http://www.me.berkeley.edu/gri\\_mech/](http://www.me.berkeley.edu/gri_mech/) (accessed February 2011).

12. Catoire, L.; Ludwig, T.; Bassin, X.; Dupr, G.; Paillard, C., *Proc. Combust. Inst.* **1998**, *27* (2), 2359-2365.
13. Catoire, L.; Chaumeix, N.; Paillard, C., *J. Propul. Power* **2004**, *20* (1), 87-92.
14. McQuaid, M. J.; Anderson, W. R.; Kotlar, A. J.; Nusca, M. J.; Ishikawa, Y., In *Proceedings of the Sixth International Symposium on Special Topics in Chemical Propulsion*, Kuo, K., Ed. 2005.
15. Wang, S. Q.; Thynell, S. T., *Combust. Flame* **2012**, *159* (1), 438-447.
16. Seamans, T. F.; Vanpee, M.; Agosta, V. D., *AIAA Journal* **1967**, *5* (9), 1616-1624.
17. Mayer, S. W.; Taylor, D.; Schieler, L., *Combust. Sci. Technol.* **1969**, *1* (2), 119-129.
18. Saad, M. A.; Sweeney, M. A.; Detweile, Mb, *Aiaa Journal* **1972**, *10* (8), 1073-1078.
19. Breisach, P.; Takimoto, H. H.; Denault, G. C.; Hicks, W. A., *Combust. Flame* **1970**, *14* (1-3), 397-403.
20. Zhao, Y.; Truhlar, D. G., *Theor. Chem. Acc.* **2008**, *120* (1-3), 215-241.
21. Tannor, D. J.; Marten, B.; Murphy, R.; Friesner, R. A.; Sitkoff, D.; Nicholls, A.; Ringnalda, M.; Goddard, W. A.; Honig, B., *J. Am. Chem. Soc.* **1994**, *116* (26), 11875-11882.
22. Jaguar, *Schrodinger, LLC, New York, NY* **2007**.
23. Valiev, M.; Bylaska, E. J.; Govind, N.; Kowalski, K.; Straatsma, T. P.; Van Dam, H. J. J.; Wang, D.; Nieplocha, J.; Apra, E.; Windus, T. L.; de Jong, W., *Comput. Phys. Commun.* **2010**, *181* (9), 1477-1489.
24. Hirata, S., *J. Phys. Chem. A* **2003**, *107* (46), 9887-9897.
25. Liu, W. G.; Dasgupta, S.; Zybin, S. V.; Goddard, W. A., *J. Phys. Chem. A* **2011**, *115* (20), 5221-5229.
26. Addison, C. C., *Chem. Rev. (Washington, DC, U. S.)* **1980**, *80* (1), 21-39.

27. Finlayson-Pitts, B. J.; Wingen, L. M.; Sumner, A. L.; Syomin, D.; Ramazan, K. A., *Phys. Chem. Chem. Phys.* **2003**, 5 (2), 223-242.
28. Liu, W.-G.; Goddard, W. A., *J. Am. Chem. Soc.* **2012**, 134 (31), 12970-12978.
29. Lai, K. Y.; Zhu, R. S.; Lin, M. C., *Chem. Phys. Lett.* **2012**, 537, 33-37.
30. Svensson, R.; Ljungstrom, E.; Lindqvist, O., *Atmos. Environ.* **1987**, 21 (7), 1529-1539.
31. England, C.; Corcoran, W. H., *Industrial & Engineering Chemistry Fundamentals* **1974**, 13 (4), 373-384.
32. Fairlie, A. M.; Carberry, J. J.; Treacy, J. C., *J. Am. Chem. Soc.* **1953**, 75 (15), 3786-3789.